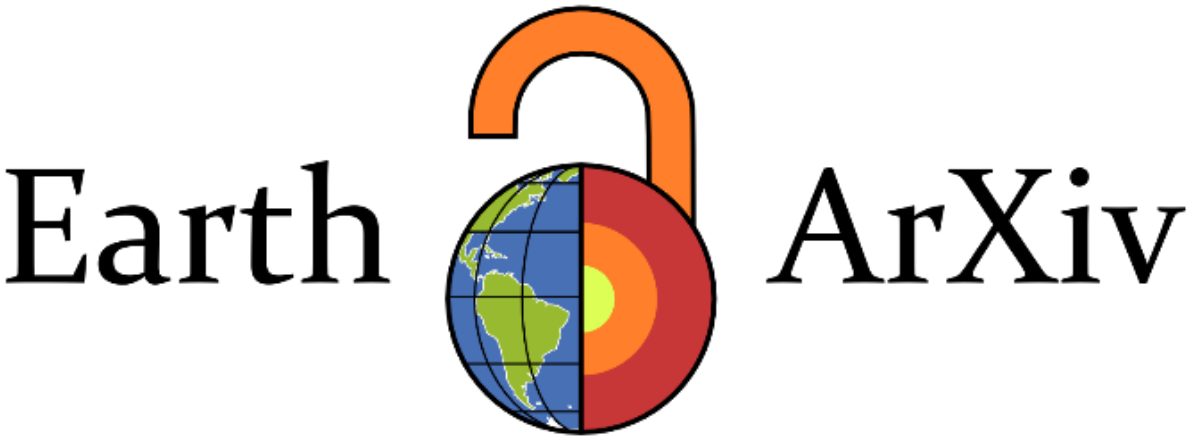

**Title:** Continental-Scale Carbonate Sedimentation and Environmental Correlates of the Shuram-Wonoka Excursion

**Authors:** *Daniel C. Segessenman[1,2] and Shanan E. Peters[2]

**Affiliations:**
1) Atmospheric, Oceanic, and Earth Sciences Department, George Mason University, Fairfax, Virginia, 22030, USA
2) Department of Geoscience, University of Wisconsin-Madison, Madison, Wisconsin, 53715, USA
*Corresponding Author: dsegesse@gmu.edu

**Abstract**

Strata of the Ediacaran Period record many Earth-Life features that distinguish the Neoproterozoic-Phanerozoic transition. However, it is difficult to determine cause and effect relationships between Ediacaran events. Continental-scale patterns of sedimentation have been used as proxies to investigate controls on Phanerozoic macroevolution, including sea level drivers and potential carbon cycling perturbations. Here we focus on quantitative properties of carbonate rock area, volume, geochemistry, and depositional environments from the North American Ediacaran System. Patterns of carbonate sedimentation and geochemistry are broadly coincident with transgressive/regressive cycles which have been linked to glacioeustacy and global/regional tectonics. Highly negative carbonate carbon isotope values distinguishing the Shuram-Wonoka carbon isotope excursion (SW-CIE) coincide with a distinct increase in carbonate quantity, which spans nearshore, outer shelf, and slope/basin depositional environments. An increase in the extent of carbonate sedimentation on the continent may indicate global marine transgression, suggesting that the excursion occurred during an interglacial warm period. This same increase in carbonate sedimentation is also broadly coincident with first occurrences of the Ediacaran biota. A subsequent increase in carbonate rock quantity in the latest Ediacaran, dominantly deposited in nearshore environments, coincides with the appearance of biomineralizers, potentially indicating common cause drivers for the extent of shallow shelves, carbonate sedimentation on the continents, and macroevolution. This analysis provides a robust, rock record-based chronostratigraphic framework within which major Ediacaran events can be anchored, new evidence of environmental correlates for several key features of the Ediacaran and provides a foundation for future hypothesis testing during the dawn of animal life.

## 1. Introduction

The Ediacaran Period is a critical transition in Earth's geological history, as reflected in its position as a boundary interval between the Proterozoic and Phanerozoic eons. The Ediacaran directly follows deglaciation of the global Cryogenian Snowball Earth glaciations; the last glaciations of great enough magnitude to cover all continents in ice sheets (Hoffman et al., 1998; Knoll et al., 2006; Hoffman and Li, 2009; Hoffman et al., 2017; Xiao and Narbonne, 2020). Ediacaran strata have been interpreted as having glacial influences, perhaps representing multiple episodes of glaciation in the mid-to-late Ediacaran (Hoffman and Li, 2009; McGee et al., 2013; Pu et al., 2016; Wang R. et al., 2023a; Wang R. et al., 2023b; Wang R. et al., 2023c; Kirshchvink, 2023; Fitzgerald et al., 2024; Wu et al., 2024). The oldest known complex macroscopic fossils that include some of the earliest metazoans, colloquially known as the Ediacaran biota, are found in mid-Ediacaran strata (Bobrovskiy et al., 2018; Xiao and Narbonne, 2020; Mussini and Dunn, 2023). The greatest magnitude negative carbon isotope ($\delta^{13}C$) excursion measured from the geologic record, known as the Shuram-Wonoka carbon isotope excursion (SW-CIE), has been identified globally from mid-Ediacaran carbonates (Burns and Matter, 1993; Grotzinger et al., 2011; Rooney et al., 2020; Xiao and Narbonne, 2020). The Ediacaran also marks the beginning of the end of the Great Unconformity, wherein there is a major increase from the latest Ediacaran to the mid-Cambrian in the quantity of preserved marine sedimentary rock in North America that was deposited on a diverse array of older Precambrian rock of many different types (Shahkarami et al., 2020; Peters et al., 2022; Segessenman and Peters, 2023; McDannell et al., 2022; Tasistro-Hart and Macdonald, 2023). Finally, the Ediacaran witnessed the final stages of the rifting of the supercontinent Rodinia, in addition to the amalgamation of Gondwana, a major transition in the Wilson supercontinent cycle (Wilson,

1966; Dewey and Spall, 1975; Schmitt et al., 2018; Condie et al., 2021; Ernst et al., 2021; Youbi et al., 2021; Nance, 2022; Macdonald et al., 2023; Müller et al., 2024). Directly following the Ediacaran and the disappearance of the Ediacaran biota, the uniquely 'explosive' Cambrian radiation of life occurs, which has its roots in latest Ediacaran evolutionary developments (Wood et al., 2019; Darroch et al., 2021; Servais et al., 2023; Segessenman and Peters, 2024). The oldest complex macroscopic fossils and high magnitude carbon isotope excursion identified from Ediacaran-age rocks globally have drawn increasing attention, both due to the appeal of working on the puzzles of extreme events and as an interval in Earth history that may be particularly informative for determining what planetary features may be important to the development of complex, macroscopic life prevalent on Earth today.

For all these reasons, the Ediacaran is a remarkable transition period in Earth history, but relatively low preserved rock quantity in comparison to the early Paleozoic (Segessenman and Peters, 2023; Bowyer et al., 2024) and a dearth of suitable index fossils for biostratigraphy makes correlating Ediacaran strata difficult (Xiao and Narbonne, 2020). New geochronologic constraints (e.g., Cantine et al., 2024; Tan et al., 2024) are being discovered and new methods for correlation (e.g. Hagen and Creveling, 2024) are being developed that seek to improve age models and our understanding of Earth systems evolution during the Ediacaran. Although studies like these are fundamental to improving our understanding of the Ediacaran, most of these approaches target key stratigraphic intervals regionally or globally and thus do not provide a full accounting of the period's complete rock record. Another approach that seeks to integrate all available stratigraphic data for a given interval in order to quantify the geologic framework and provide additional constraints on the nature of sampling and changes in the Earth system is macrostratigraphy (Peters, 2006; Peters and Husson, 2018; Peters et al., 2018; Peters et al., 2022;

Segessenman and Peters, 2023; Quinn et al., 2024). This approach has enabled quantitative analyses of continental sedimentation patterns and their geodynamic drivers (e.g., Phanerozoic Sloss sequences; Tasistro-Hart and Macdonald, 2023), analysis of relationships between igneous rock area and detrital zircon ages (Peters et al., 2021), examinations of correlations between rock quantity and biodiversity (e.g., Peters and Heim, 2011; Husson and Peters, 2017; Zaffos et al., 2017), and more (Peters et al., 2022). Of the rock types examined, macrostratigraphic quantities of carbonate have been identified as particularly useful for analyzing drivers of continental scale stratigraphic patterns.

Macrostratigraphic changes in carbonate quantity have been used as a proxy for continental flooding and to help constrain how Earth-life systems co-evolve (Valentine and Moores, 1970; Wilkinson and Walker, 1989; Peters, 2006; Peters, 2008; Hannisdal and Peters, 2011; Segessenman and Peters, 2023; Boulila et al., 2023; Alcott et al., 2024). Recently, stratigraphic data was compiled and developed for an Ediacaran-centric 'mesostratigraphic' framework, a focused macrostratigraphic approach in which only Ediacaran-age strata and rocks chronostratigraphically above and below were compiled from across North America, Central America, Greenland, and Svalbard (Segessenman and Peters, 2023). This analysis yielded additional perspectives on rock quantity and demonstrated that Ediacaran events are anchored within a shifting rock record that is responding to changes in the Earth system. For example, increases and decreases in the quantity and proportion of carbonates in the Ediacaran suggested a potential Sloss sequence-like cycle in the Ediacaran, which coincided with the SW-CIE (Segessenman and Peters, 2023) and biodiversity patterns (Segessenman and Peters, 2024). A previous depositional environment analysis of key Ediacaran carbonate sections globally found that the SW-CIE coincided with global transgression (Busch et al., 2022) and these authors

concluded that the SW-CIE may have been a shallow marine focused result of enhanced primary productivity and/or evaporative processes that decoupled carbonate environments from global oceanic dissolved inorganic carbon (DIC).

There are numerous studies that propose mechanisms that do not require shifts in oceanic DIC to produce the globally occurring, extremely negative $\delta^{13}C$ values that are the signature of the SW-CIE in Ediacaran carbonates (e.g., Grotzinger et al., 2011; Schrag et al., 2013; Shields et al., 2019; Husson et al., 2020; Laakso and Schrag, 2020; Li et al., 2020; Xu et al., 2021; Busch et al., 2022; Cui et al., 2022; Shi et al., 2023; Wang W. et al., 2023). This is largely due to the SW-CIE reaching values far lower than the assumed -5‰ of volcanic $CO_2$ input and the SW-CIE's apparent multi-million year duration (Rooney et al., 2020; Cantine et al., 2024; Hagen and Creveling, 2024) which greatly exceeds the residence time of carbon in Earth's oceans (~0.1 m.y.) and breaks the carbon isotope mass balance of standard global carbon cycling models (Kump and Arthur, 1999; Busch et al., 2022). However, carbon cycling perturbation of oceanic DIC and mechanisms that could have decoupled shallow marine carbonate $\delta^{13}C$ need not be mutually exclusive. Geologic evidence for Laurentian rifting and a pulse of the Central Iapetus Magmatic Province (CIMP) coincides with the currently constrained interval for the SW-CIE (Condie et al., 2021; Youbi et al., 2021; Macdonald et al., 2023). The SW-CIE is stratigraphically bracketed by glacially influenced sedimentary rocks of the Gaskiers (below) and Luoquan/Hankalchough (above), suggesting a potential connection to climate and/or glacioeustacy (Wang R. et al., 2023b; Wang R. et al., 2023c; Fitzgerald et al., 2024; Wu et al., 2024). Assembly of the supercontinent Gondwana begins in the latest Cryogenian and reaches peak preserved orogen length during the mid-to-late Ediacaran (Meert and Lieberman, 2008; Ganade de Araujo et al., 2014; Oriolo et al., 2017; Schmitt et al., 2018; Condie et al., 2021;

Murphy et al., 2024). Large Igneous Province (LIP) emplacement, supercontinent assembly and breakup, and glaciations are mechanisms that have all been tied to Phanerozoic perturbations in oceanic DIC $\delta^{13}C$ and macroevolution (e.g., Kump and Arthur, 1999; Isson et al., 2019; Cramer and Jarvis, 2020; Condie et al., 2021; Green et al., 2022; Tian and Buck, 2022; Boulila et al., 2023).

Globally effective tectonic mechanisms known to have contributed to carbon cycling perturbation in Earth's past appear to have been active during the Ediacaran, but questions of specifically when they were active and the significance of their contribution to global environmental change remain. Here we present an updated mesostratigraphic compilation and analysis of Ediacaran carbonate quantity, depositional environments, and geochemistry from across the North American continent. The goal is to provide a comprehensive, quantitative dataset on Ediacaran stratigraphy, as currently represented in the published literature, that can be updated and adjusted as future research expands our understanding. Although this compilation and analysis cannot overcome the long-standing challenges of geochronology in the latest Neoproterozoic, it does provide a rock-based chronostratigraphic framework from which we can anchor evidence of significant Ediacaran events and potentially provide new perspectives on Earth systems evolution at the dawn of complex macroscopic life.

## 2. Methods

Bounding ages, thicknesses, lithologies, and proportional positions of 5,559 carbon isotope measurements within 548 Ediacaran age rock units were derived from the 'mesostrat' dataset of Segessenman and Peters (2023), with an additional 3,403 carbon isotopes compiled from multiple sources for this study. See Supplementary Table S1 and S2 for all compiled carbon

isotope measurement data, including measured values, stratigraphic positions, references, and locations. Carbon isotope measurements were assigned ages based on their relative stratigraphic position within an age model that was constructed for the Ediacaran System in NA (for a complete description of the age model construction, see pages 401-404 of Segessenman and Peters, 2023). Construction of the age model involved assigning each rock unit a chronostratigraphic bin based on the published literature and then interpolating all unit boundary positions within that chronostratigraphic bin using super-positional constraints. This step was then followed by adjustments based on available radioisotopic data and regional correlations. Carbon isotope measurements were not directly used to construct the age model, though published age interpretations have been influenced by chemostratigraphic correlations. Several adjustments to Ediacaran rock unit bounding ages from Segessenman and Peters (2023) were made here to incorporate updates from studies published after the completion of the original mesostrat dataset (e.g., Busch et al., 2023; Ineson et al., 2024).

Carbonate-bearing stratigraphic units and associated $\delta^{13}C$ and $\delta^{18}O$ measurements were assigned to one of three marine depositional environments based on available interpretations (largely associated with interpreted depths of carbonate environments) in the literature: 1) shoreface to shallow shelf (nearshore); 2) non-nearshore continental shelf (outer shelf); and 3) continental slope to basin settings (slope/basin). This approach is similar to the environmental analysis of Busch et al. (2022), though with a coarser resolution encompassing all Ediacaran-age rocks across North America. A full list of Ediacaran carbonate bearing rock units, their associated environmental interpretation, and the primary reference for depositional environment interpretations is shown in Table 1. If no depositional environment interpretation was available in the literature, carbonate units were assigned to a general ‘inferred marine’ category. The

primary carbonate phase (dolomite/calcite) of each measured isotope value was included when available. All compiled $\delta^{13}C$ and $\delta^{18}O$ data used for this study are included in the supplement (Table S1).

From the updated dataset of Ediacaran rocks, compiled carbon and oxygen isotope measurements, depositional environment interpretations, and quantities of rock were expressed as a time series. Area and volume flux (sum of thickness times column area divided by rock unit duration) were the primary quantities calculated as time series and were divided into categories of: 1) carbonate depositional environments (as listed above), 2) total carbonates, 3) total siliciclastics, 4) dolostone only, and 5) limestone only. Rock units with multiple lithologies were split into lithologic categories based on the relative proportion of each lithology recorded for that rock unit. All rock quantity values have a 3 m.y. smoothing applied, which is on the order of the expected minimum error in the age model. Raw carbon isotope values, categorized by depositional environment and phase, were then plotted with the calculated rock quantities, using the same integrated age model. Next, 5 m.y. moving window averages (with 3 m.y. smoothing) of carbon and oxygen isotope values were calculated by locality, phase, and depositional environment. For each moving window average of carbon and oxygen isotopes, an average value for each locality was calculated first to avoid overweighting localities with higher numbers of samples. Correlations between $\delta^{13}C$ and $\delta^{18}O$ values, categorized by depositional environment, were calculated using Spearman's $\rho$ with a 5 m.y. moving window. 2 standard deviation error bars and envelopes were calculated for carbon/oxygen isotope averages and the $\delta^{13}C/\delta^{18}O$ correlations using block bootstrap resampling. Overlays highlighting potentially relevant Ediacaran Period events (e.g. Gaskiers glaciation, advent of calcifying taxa, etc.) were added to each of the time series with timings based on current interpretations in the published literature.

196

197 **3. Results**

198 Ediacaran rock-bearing column areas (shown as polygons) in North America, Greenland,
199 and Svalbard, with those bearing carbonates and geochemical analyses highlighted, are shown in
200 Figure 1. The Ediacaran record of North America is limited to the highly deformed remnants of
201 the ancient margins of Laurentia, except for terranes in SE Canada and NW United States that
202 are interpreted as either peri-Gondwanan or peri-Baltican volcanic arcs accreted to Laurentia
203 during the Paleozoic (Beranek et al., 2023; Murphy et al., 2023; Keppie and Keppie, 2024). The
204 majority of North America's Ediacaran age carbonate rock is found along its western margin,
205 and, consequently, most geochemical analyses are also found in those regions (NW Canada, SW
206 U.S.A., and NW Mexico). The locations, primary references, approximate stratigraphic
207 positions, and reported values of geochemical analyses used for this study are available in the
208 supplementary information associated with this study (Supplementary Tables S1-2).

209 North American Ediacaran carbonate area and volume exhibit similar trends and are
210 largely interchangeable metrics for rock quantity in this study. Ediacaran carbonate quantity
211 starts off relatively high in the earliest Ediacaran, particularly among shallow environments, a
212 feature indicative of post-Marinoan deglaciation and cap carbonate deposition (Figure 2A-B).
213 Carbonate quantity drops off sharply post cap carbonate deposition and remains low in all
214 environments until a stepwise increase at ~590 Ma. Between 585-580 Ma there is sharp increase
215 in carbonate quantity of all environments, but particularly in the slope/basin, that culminates in
216 the greatest area and volume flux of Ediacaran carbonate, between 580 and 570 Ma. Following
217 this maximum, there is a sharp decrease to a local minimum by 565 Ma. Another sharp increase
218 and decrease in carbonate quantity occurs between 562 and 555 Ma, before another sharp

219 decrease between 555 and 550 Ma. The second increase is largely driven by slope/basin
220 environments for volume flux and among shelf carbonates for area. This is followed by a final
221 increase in carbonate quantity, driven primarily by shallow carbonates between 550 and 545 Ma,
222 which then sharply decrease to pre-590 Ma values during the terminal Ediacaran (Figure 2A-B).
223 Carbonates represent the greatest proportion of total sedimentary rock quantity during the
224 deposition of cap carbonate in the earliest Ediacaran and during the 580-570 carbonate quantity
225 maximum (Figure 2A-D).

226 Carbon isotope values ($\delta^{13}C$) associated with cap carbonate deposition during the earliest
227 Ediacaran are highly variable, ranging from ~8‰ to as low as -11‰ (Figure 1A). Between 620
228 Ma and 595 Ma there are relatively few carbon isotope measurements available, due in part to
229 the decreased quantity of carbonates (and sedimentary rock in general) during this interval. A
230 highly negative cluster of slope/basin carbon isotope values at 610-600 Ma are from carbonates
231 of the Geikie Siding Mbr of the Old Point Fort Fm, which has a date of 607.8 ± 4.7 Ma (Kendall
232 et al., 2004; Cochrane et al., 2019). At ~595 Ma, carbon isotope measurements become more
233 abundant, coincident with the initial stepwise increase of carbonate quantity (Figure 1A). From
234 595-575 Ma, carbon isotope values in all three environment categories exhibit significance
235 variance but steadily increase values as high as +11‰, before precipitously decreasing to values
236 as low as -16‰; this shift is coincident with the carbonate volume and area maximum observed
237 from 580-565 Ma (Figure 1A). From the excursion nadir at ~572 Ma, carbon isotope values
238 climb to values ranging between about +4‰ and -4‰. The climbing positive values, sharp
239 decrease to extremely negative values, and subsequent increase to more positive/stable values
240 between 585 and 565 Ma is the signature of the SW-CIE. The excursion is bracketed by
241 hypothesized glaciations of the Gaskiers and the Luoquan/Hankalchough, coincident with an

episode of higher activity Laurentian rifting, positioned within the proposed timeframe for the Ediacaran ultraweak magnetic field event (Bono et al., 2019; Domeier et al., 2023; Huang et al., 2024), and coincides with the appearance of the oldest complex macroscopic fossils of the Ediacaran biota (Figure 1A). Carbon isotope values hold relatively steady for the remainder of the Ediacaran, although with an overall decreasing trend and a possible negative excursion (only from shallow marine carbonates) at 550-545 Ma that coincides with the second and final carbonate quantity increase and the advent of Ediacaran calcifying taxa (Figure 1A).

Carbonate rock quantities, separated by their dominant carbonate type (dolostone or limestone), exhibit departures from the aggregate carbonate record (Figure 3A-E). Limestone is rare to non-existent from the earliest Ediacaran to 590 Ma (Figure 3B,D). Shallow marine dolostone makes up the majority of this early record, including that of the cap carbonate (Figure 3C,E). Both limestone and dolostone quantities increase at ~585 Ma, though dolostone quantities are more pronounced between 580 and 565 Ma. Slope/basin carbonates are the largest contributor to the volume flux of both limestone and dolostone within the Shuram-Wonoka interval. Dolostone associated with all three environmental categories makes up the largest proportion of carbonate area within the Shuram-Wonoka interval. The second pulse of carbonate volume flux from 565-555 Ma is dominated by limestone and slope/basin environments. The final pulse of carbonate quantity from 550-545 Ma is evenly distributed between dolostone and limestone, predominately deposited in shallow marine environments.

Averaged Ediacaran carbon isotope values separated by locality, phase, and environment largely follow the overall trends observed in the aggregate values, though there are some differences. Average carbon isotope values are between 0 and -4‰ during the earliest Ediacaran and remain relatively steady until around 620 Ma, when error increases and averaged carbon

isotope values fluctuate due to the paucity of carbonate-bearing units (Figure 4A-C). At ~595 Ma, values stabilize as the number of localities with carbonate increases and exhibit increasingly positive values before the precipitous decrease to the very negative values (<-6‰) that define the SW-CIE between 580 and 565 Ma. Carbon isotope values increase to around 0‰ by ~565 Ma and then show a slight downward trend for the rest of the Ediacaran, with a potential negative excursion after 545 Ma (Figure 4A-C).

Carbon isotope values averaged by locality exhibit similar overall trends, but with differing magnitudes. Some localities do have anomalously high values in the Shuram interval (Virginia and SW Canada), though the sections bearing these measurements also have greater stratigraphic and positional uncertainties within the age model (Figure 4A). Averages of carbon isotopes separated by reported carbonate phases follow the same general trends, but dolomite averages do not reach positive values (+6‰ maximum) as great as those of calcite (+9‰ maximum). Calcite values also appear to be more negative than dolomite within the Shuram-Wonoka interval (-9‰ for calcite vs. -6‰ for dolomite). Thus, the magnitude of the paired positive-negative excursion of the Shuram-Wonoka is typically more attenuated in dolomite samples (Figure 4B). Carbon isotope values averaged by environmental categories exhibit similar overall trends, though the slope/basin setting appears to have a delayed positive increase compared with nearshore and middle/outer shelf samples (Figure 4C). Averaged values of all three environmental categories reach similarly negative values within the Shuram-Wonoka interval (-7‰ minimum), suggesting a ubiquitous shift across carbonate depositional environments (Figure 4C).

Correlations between $\delta^{13}C$ and $\delta^{18}O$ in all three environmental categories exhibit moderate ($\boldsymbol{\rho}$ >=0.5) to strong ($\boldsymbol{\rho}$ >= 0.75) positive correlation in the earliest Ediacaran. This

correlation decreases but can't be calculated after 620 Ma due to insufficient data (Figure 4D). All environmental categories have sufficient data by 575 Ma, and all environmental categories exhibit increases in $\delta^{13}C$ and $\delta^{18}O$ correlations from weak/no ($\boldsymbol{\rho}$ = 0 to 0.25) to moderate and strong positive within the Shuram-Wonoka interval. Correlations fluctuate but generally decrease to weak ($\boldsymbol{\rho}$ <= -0.25) and moderate negative correlations ($\boldsymbol{\rho}$ <= -0.5) after 565 Ma and increase to weak positive correlations by the end of the Ediacaran (Figure 4D).

Carbonate oxygen isotope values ($\delta^{18}O$) were analyzed by environment, locality, and phase using the same methods applied to carbon isotope values (Figure 5). With some exceptions, Ediacaran carbonate $\delta^{18}O$ generally fluctuates within a range of 0 to -15‰. When separated by relative environmental category, nearshore carbonate $\delta^{18}O$ is generally more positive on average than the outer shelf or slope/basin settings, with the exceptions of the early Ediacaran (low data availability) and a sharp decrease at ~562 Ma near the onset of proposed Luoquan/Hankalchough glaciation onset (Figure 5B). Interestingly, nearshore $\delta^{18}O$ values exhibit a similar trend to their $\delta^{13}C$ counterparts within the SW-CIE (climb to more positive values pre-Shuram, extended decrease within Shuram, post-Shuram rise to more positive values), while outer shelf and slope/basin values vary less and do not follow this trend (Figures 4C; 5B). As might be expected, $\delta^{18}O$ varies between localities, though a couple of features stand out: 1) NW Canada, Death Valley, and Svalbard localities show relatively greater agreement in the earliest Ediacaran than at any other time in the Ediacaran, and 2) the nearshore Shuram-Wonoka trend in $\delta^{18}O$ mainly mirrors that of the Death Valley region (Figure 5C). $\delta^{18}O$ averaged by carbonate phase (calcite and dolomite) are relatively stable, follow similar trends, but exhibit distinct values during the early Ediacaran (Figure 5D); dolomite is consistently more positive by ~3‰ during intervals with greater amounts of data. Both phases then track similarly through the

low data interval, with a significant decrease largely reflecting trends from SW Canada (Figure 5D). Both phases have a Shuram-like trend coincident with that of $\delta^{13}C$ (~580-565 Ma), however, calcite has a greater magnitude decrease immediately before the Shuram that coincides with the Gaskiers glaciation and the Shuram-like excursions of dolomite and calcite are offset temporally. After the Shuram, calcite and dolomite average values separate as in the early Ediacaran (dolomite more positive than calcite) but both phases fluctuate more, with calcite in particular exhibiting larger fluctuation between -9‰ and -18‰ (Figure 5D).

## 4. Discussion

The Ediacaran System is uniquely positioned as a transition interval between a protracted period of rather low preserved sediment quantity and markedly higher sediment abundance starting in the Cambrian, a prominent transition in the rock record marked in many places by the Great Unconformity (Peters et al., 2018; Shahkarami et al., 2020; Ma et al., 2022; McDannell et al., 2022; Segessenman and Peters, 2023, Tasistro-Hart and Macdonald, 2023). The ancient Laurentian margins on which Ediacaran sedimentary rocks were deposited have been deformed and dissected by a variety of distinct tectonic events (e.g., Ma et al., 2023; Macdonald et al., 2023; van Staal and Zagorevski, 2023; Weil and Yonkee, 2023). The North American Ediacaran record (particularly that of the east coast) is also a composite record of ancient Laurentian continental margins and accreted peri-Gondwanan or peri-Baltican volcanic arc terranes (Beranek et al., 2023; Murphy et al., 2023; Keppie and Keppie, 2024). Existing geochronologic constraints for Ediacaran stratigraphy are limited (relative to the Phanerozoic), not due to a lack of effort, but due to generally limited availability of accessible Ediacaran outcrop, conventionally dateable material, and traditional biostratigraphic controls (Xiao and Narbonne, 2020).

As an additional challenge, all Ediacaran sedimentary rocks have experienced some degree of diagenesis and/or tectonic deformation, and many latest Neoproterozoic age rocks, particularly those from the SE United States, are well categorized as metasedimentary (e.g., Thomas, 1991; Hatcher, 2010; Waldron et al., 2019). Nevertheless, a wide range of studies have made considerable progress towards understanding these rocks (e.g., Canfield et al., 2020; Rooney et al., 2020, Busch et al., 2022; Bowyer et al., 2024; Cantine et al., 2024; Wei et al., 2024). The North American compilation of Ediacaran stratigraphy used here (Segessenman and Peters, 2023) was constructed with the intent to represent the aggregated Ediacaran system as it stands in the published literature. Marine carbonate quantity, presence/absence, and geochemistry have all been interpreted as reflecting various local and global-scale geologic processes during the Phanerozoic (e.g., Ahm and Husson, 2022; Peters et al., 2022; Segessenman and Peters, 2023; Hohmann et al., 2024), and we apply that same general methodology here. Our compilation generally agrees with other published summaries (e.g., Fig. 2 of Macdonald et al., 2023; Bowyer et al., 2024; Cantine et al., 2024), although we acknowledge that our understanding of all rocks everywhere is subject to change as new studies of them unfold.

### 4.1 Geologic Context of Ediacaran System Carbonates

A recent study that simulated carbonate records to determine how preservation affected interpretations of macroevolution by Hohmann et al. (2024) found that rarer, prolonged unconformities were more influential than the degree of stratigraphic completeness on recovering and interpreting ‘true’ macroevolutionary trends. They concluded that stratigraphic sections that are incomplete but have more regular hiatus frequency/duration enable recovery of macroevolutionary trends and that understanding processes that can influence stratigraphic

architecture are critical for interpretation of macroevolution. This suggests that it is possible for process signals to be recovered from the aggregated Ediacaran stratigraphic record despite its decreased preservation relative to the Phanerozoic. Based on current correlations of the Ediacaran across Laurentia, periods of widespread hiatuses within the sections where the Ediacaran is preserved are between ca. 600-590 Ma, ca. 562-555 Ma, and across the Ediacaran-Cambrian boundary (see Figure 2 in Macdonald et al., 2023; Segessenman and Peters, 2023; Bowyer et al., 2024). Furthermore, the nature of the Ediacaran's upper boundary with the Cambrian suggests a relatively narrow timeframe for potential focused erosion of Ediacaran strata during the Phanerozoic.

Although there is a globally recognized hiatus commonly present at the Ediacaran-Cambrian boundary (Shahkarami et al., 2020; Bowyer et al., 2022; Bowyer et al., 2024), Ediacaran sedimentary sequences are generally overlain by Cambrian marine sediments (Segessenman and Peters, 2023; Bowyer et al., 2024). It is rare that an Ediacaran sedimentary sequence is overlain by sedimentary sequences younger than Cambrian, in that essentially everywhere Ediacaran age sedimentary rocks are preserved, they were sealed by the deposition of Cambrian sedimentary rocks across the Ediacaran-Cambrian transition. This observed relationship between the Ediacaran and Cambrian Systems suggests that the decreased quantity of preserved rock in the Ediacaran (relative to the following Paleozoic; Segessenman and Peters, 2023) is less a signal of erosion of a formerly much more extensive Ediacaran sedimentary rock record, but is instead an indication of limited accommodation and lack of sedimentation on the continents to begin with. The proportion of the preserved sedimentary record that is carbonate (Fig. 2), which is primarily driven by base-level associated accommodation on continental margins (Miall, 2016), reinforces this view. We interpret this as an indication that the changes in

North American Ediacaran carbonate quantity are representative primarily of 2nd order ($10^7$ yr) to 3rd order ($10^6$ yr) scale changes in epicontinental marine deposition reflecting a combination of local and global geologic processes.

### 4.2 Cap Carbonate Deposition

The base of the Ediacaran is marked by the appearance of a global cap carbonate that represents deglaciation at the end of the Cryogenian snowball Earth episodes (Hoffman et al., 1998; Knoll et al., 2006). Models suggest a rapid transition from snowball Earth conditions in the latest Cryogenian to a 'supergreenhouse' state as volcanically sourced atmospheric $CO_2$ exceeded the threshold to initiate global glacial retreat and resulted in rapid transgression on continental margins (Creveling and Mitrovica, 2014; Myrow et al., 2018). The extreme hothouse conditions are thought to have led to an oversaturation of $CO_2$ in the ocean-atmosphere system, ultimately leading to the deposition of the distinctive cap carbonate that marks the base of the Ediacaran (Sun et al., 2022). Cap carbonate deposition on Laurentia can be recognized by the elevated quantity of carbonate rock (dominantly dolostone; Fig. 3B-E) preserved in the earliest Ediacaran and that the earliest Ediacaran record has the greatest proportion (nearly 50%) of sedimentary rock units that contain carbonate (Figs. 2, 3). While the proportion of the Ediacaran marine sedimentary record that contains carbonate decreases throughout the Ediacaran, cap carbonate sequences do not represent the greatest Ediacaran quantity of carbonate material in Laurentia, a result that is contrary to what might be expected (Fig. 2).

Sections that definitively preserve the earliest Ediacaran on North America are rare, even when considering the Ediacaran's overall decreased preserved rock quantity. Carbonate quantity in the earliest Ediacaran of Laurentia is largely represented by the Noonday Dolomite in the SW

403 contiguous USA, the Hayhook and Ravensthroat formations from NW Canada, the Katakturuk
404 Dolomite from NE Alaska, the base of the Dracoisen Formation in Svalbard, and the Canyon
405 Formation from East Greenland. With the exceptions of the Katakturuk and Noonday Dolomite
406 formations, cap carbonate formations of North America are thin, generally <20m thick (Fairchild
407 and Hambrey, 1995; Macdonald et al., 2009; Macdonald et al., 2013; Creveling et al., 2016).
408 Despite representing the highest proportion of the sedimentary record that contains carbonate at
409 any time in the Ediacaran, the relative rarity and generally short-lived stratigraphic expression of
410 the Ediacaran cap carbonate in North America explains why its estimated area and volume are
411 eclipsed by that of the mid-Ediacaran Shuram interval, in which the frequency of carbonate
412 bearing sections increases across a higher number of stratigraphic sections with larger areas and
413 greater thicknesses (Fig. 2C-D).
414 Based on projections of the terminal Cryogenian deglaciation's effect on sea level
415 (Creveling and Mitrovica, 2014; Myrow et al., 2018), it is not particularly surprising that the
416 carbonate area and volume increases in the earliest Ediacaran are largely associated with
417 nearshore environments, though isotopic sampling captures all three environmental categories in
418 the earliest Ediacaran on North America (Figs. 2-5). The dominance of dolostone and strong to
419 moderate positive correlations ($\rho >= 0.75$ and 0.5 respectively) between $\delta^{13}C$ and $\delta^{18}O$ from all
420 environmental categories (Figs. 3E,4D) in the earliest Ediacaran suggests potential diagenetic
421 influences and/or increased ocean alkalinity, which is consistent with high resolution global
422 geochemical analyses and interpretations of the earliest Ediacaran cap carbonate (Hoffman,
423 2011; Ahm et al., 2019; Sun et al., 2022). High variance of raw carbon isotope values (+8 to -
424 7‰) during the earliest Ediacaran is another well documented observation attributed to local
425 diagenetic effects (Ahm et al., 2019), although average $\delta^{13}C$ values categorized by phase and by

environment remain strikingly close (within 1-2‰) of each other before diverging and exhibiting more variance for the rest of the Ediacaran (Fig. 2B-C). In contrast, $\delta^{18}O$ values are distinctly separate when categorized by phase and environment in the earliest Ediacaran (Fig. 5B,D), exhibiting the mass balance modeled expectation of an ~3‰ difference between the calcite and dolomite phases (Land, 1980; Swart, 2015). These results are consistent with globally observed and analyzed features from the earliest Ediacaran, including the estimated proportion of the sedimentary record that is carbonate. The intriguing result here is that the carbonate proportion is at a maximum in the earliest Ediacaran and continuously declines (with fluctuations) throughout the remainder of the period, even though siliciclastic flux doesn't significantly increase until the mid-Ediacaran (Fig. 2C-D). This could reflect overall decreasing oceanic carbonate saturation throughout the Ediacaran as carbonates were deposited in the limited accommodation on continental margins and/or a general drowning of carbonate environments by increased siliciclastic input, with exceptions for pulses of increased carbonate preservation, such as during the SW-CIE (Fig. 2).

### 4.3 Early Ediacaran low preserved rock interval

The post-cap carbonate early Ediacaran sedimentary record from North America is sparsely represented (Figs. 2-5) by thicker, long-ranging rock units, such as the Sheepbed Fm from NW Canada, the undifferentiated lower Johnnie Fm of the SW USA, the Dracoisen Fm of Svalbard, the Morænesø Fm from northern Greenland, and the Canyon Fm from east Greenland (see references in Segessenman and Peters, 2023). This interval includes the lowest counts of distinct marine sedimentary units observed during the Ediacaran and low preserved rock volume/area (Fig. 2). Interestingly, the proportion of sedimentary rock that is carbonate

fluctuates, but consistently decreases through this interval, as it appears to do for the entire Ediacaran Period (Fig. 2D). The low (and sometimes non-existent) amount of preserved carbonate and few geochronologic constraints explains the low number of isotopic analyses in this interval and the increase in the error envelope for isotopic averages (Figs. 4,5). The apparent excursion from ~610-600 Ma is due to isotopic measurements from the Old Fort Point Fm of SW Canada, which bears an early Ediacaran Re-Os date of 607.8 ± 4.7 Ma (Kendall et al., 2004; Cochrane et al., 2019). A lower Ediacaran (from cap carbonate to ~590 Ma) hiatus appears to be a common feature of the Ediacaran System on multiple continents, suggesting a potential global driver of low rock preservation during this interval (Cantine et al., 2024; Li et al., 2024). Despite the lack of data, the general absence of preserved rock during this often greater than 40 m.y. interval is interesting in and of itself and may indicate geologic processes that contributed to the lack of rock preserved from this time (Miall, 2016). More specifically, limited accommodation for sediments on continents (Segessenman and Peters, 2023), reverse weathering processes (Isson and Planavsky, 2018; Zheng et al., 2024) and outgassing from Laurentian rifting, and/or early pulses of CIMP magmatism (Ernst et al., 2021; Macdonald et al., 2023) could have maintained elevated $pCO_2$ (and therefore a more erosive period) in a warm/hothouse following Marinoan deglaciation. Conversely, increasing orogenic activity (Schmitt et al., 2018; Condie et al., 2021; Müller et al., 2024) and associated $pCO_2$ drawdown may have driven an overall cooler climate and decreased rates of erosion (outside of Gondwanan orogenic zones) during the early to middle Ediacaran (Fan et al., 2025).

### 4.4 Mid-Ediacaran rock quantity increase, Gaskiers glaciation, and the SW-CIE

The end of the low preserved rock interval, indicated by the rising limb of preserved siliciclastic and carbonate quantity at ~585 Ma, coincides with strata containing evidence of the Gaskiers glaciation (Fig. 2). The increase in preserved sediment quantity is opposite of what is generally expected during a glacial interval, but we attribute this rock quantity increase to Laurentian specific tectonic controls, such as continental margin subsidence and rift-associated accommodation (Busch et al., 2022; Segessenman and Peters, 2023). Evidence of glaciation in the Gaskiers Fm had been tightly constrained to a timeframe of ~340 kiloyears between 579.63 ± 0.15 and 579.88 ± 0.44 Ma (Pu et al., 2016). However, recent studies of the underlying Mall Bay Fm suggest a longer-term onset and duration for the Gaskiers glaciation (Fitzgerald et al., 2024). The overall geographic distribution and duration of globally occurring upper Ediacaran glacial intervals is an area of continuing research and geochronologic constraints that provide exact timings of Ediacaran strata interpreted as bearing glacial influences are rare, which allows for multiple models of mid-late Ediacaran glaciation (Kirschvink, 2023; Wang R. et al., 2023b; Wang R. et al., 2023c; Wu et al., 2024). Despite the difficulty in establishing a robust temporal framework, glacially influenced strata occur stratigraphically above and below carbonates bearing the highly negative $\delta^{13}C$ values of the SW-CIE, suggesting that there are glacial periods before and after the excursion, but as of yet, no definitive constraints have placed glaciation as coeval with the SW-CIE (Wang R. et al., 2023c, Fitzgerald et al., 2024, Wu et al., 2024). There do not appear to be any significant changes in $\delta^{13}C$ or carbonate quantity directly associated with the Gaskiers glaciation, although there are apparent negative excursions in outer shelf and slope/basin average $\delta^{18}O$ values that coincide with a positive $\delta^{18}O$ trend in the nearshore, which may suggest a response of carbonate $\delta^{18}O$ to glaciation/deglaciation during this interval (Figs. 2-5). $\delta^{18}O$ is thought to increase during glacial periods and decrease during deglaciation (Swart,

2015), so their coincidence may reflect age model inaccuracies. The $\delta^{18}O$ value of carbonates is also considered to be much more susceptible to diagenetic effects, so ultimately these apparent trends may be coincidental. While there do not appear to be clear trends in carbonate geochemistry or quantity associated with the Gaskiers glaciation, the proposed end of the Gaskiers does appear to be associated with the much more distinctive signals of the SW-CIE.

Carbonates bearing the SW-CIE were deposited within transgressive systems tracts globally (Busch et al., 2022) and analyses of global Ediacaran sedimentary rock quantities from key stratigraphic sections have suggested increased sedimentary rock accumulation rates and an increased flux of previously limited elements (e.g., sulfate and phosphorus) from terrestrial environments starting in the mid-Ediacaran (Cantine et al., 2020; Dodd et al., 2023; Segessenman et al., 2023; Walton et al., 2023; Wang H. et al., 2023; Bowyer et al., 2024; Cantine et al., 2024). Mid-Ediacaran carbonate area and volume increases in all environmental categories across Laurentia and compiled $\delta^{13}C$ measurements categorized by phase and depositional environment exhibit similarly negative trends for the SW-CIE (Figs. 2-4). The duration of the SW-CIE, assuming it is a synchronous signal, has been constrained to be on the order of 5 million years or less (Cantine et al., 2024; Hagen and Creveling, 2024). The length of the excursion, its direct coincidence with stratigraphic evidence suggesting a continental-scale flooding sequence (Busch et al., 2022; Segessenman and Peters, 2023; Bowyer et al., 2024; Segessenman and Peters, 2024), and its stratigraphic bracketing by glacially influenced strata suggests the possibility that the SW-CIE could represent an interval of warming between two intervals of glaciation, similar to that of the Trezona anomaly (albeit with potentially less extreme glaciation), which is measured from carbonates deposited after Sturtian deglaciation but before the Marinoan glaciation (Halverson et al., 2020; Ahm et al., 2021).

Many studies have provided hypotheses explaining the SW-CIE's extreme magnitude in ways that obviate the need for classic drivers (e.g., enhanced $CO_2$ outgassing) of major perturbations to the carbon cycle and oceanic DIC (e.g., Derry, 2010; Schrag et al., 2013; Lee et al., 2015; Cui et al., 2017; Shields et al., 2019; Cao et al., 2020; Cui et al., 2022; Wang H. et al., 2023; Gu et al., 2024) due to the potential for sampling bias in a geologic period with decreased rock preservation (Husson et al., 2020; Busch et al., 2022; Segessenman and Peters, 2023) and difficulties in applying Phanerozoic carbon cycling and isotope mass balance models (e.g., Kump and Arthur, 1999) to a seemingly multi-million year, high magnitude CIE (Grotzinger et al., 2011; Gong and Li, 2020; Rooney et al., 2020; Busch et al., 2022; Cantine et al., 2024; Hagen and Creveling, 2024; Tan et al., 2024). However, longstanding geologic evidence indicates that there are several global-scale geologic mechanisms operating in the latest Neoproterozoic that could be associated with carbon cycling perturbations (as recognized by others, e.g., Caxito et al., 2021; Cui et al., 2021; Youbi et al., 2021; Busch et al., 2022), including the final stages of Rodinia rifting and associated LIP emplacements of the Central Iapetus Magmatic Province (Youbi et al., 2021; Macdonald et al., 2023; Müller et al., 2024), initiation of the Gondwanan supercontinent amalgamation (Oriolo et al., 2017; Schmitt et al., 2018; Condie et al., 2021), and the Acraman mid-Ediacaran bolide impact crater (with estimated impact energy great enough to exceed theoretical global catastrophe threshold), which has been associated with turnover in Ediacaran primary producers (Williams and Schmidt, 2021; Figs. 2-5; Table 2). These potential mechanisms for carbon cycling perturbation need not be mutually exclusive with existing hypotheses explaining the extreme magnitude of the SW-CIE, but rather provide potential mechanisms for decreasing oceanic DIC $\delta^{13}C$ that could have been modified by factors unique to mid-Ediacaran oceans (e.g. enhanced organic matter oxidation, increased sulfate flux,

microbial mediation, evaporation on shallow shelves etc.), leaving a global carbonate $\delta^{13}C$ signal that represents a complex mix of factors. Although post-burial diagenesis as a primary driver of SW-CIE $\delta^{13}C$ values (Derry, 2010) is now considered unlikely (e.g., Husson et al., 2020; Cui et al., 2021; Busch et al., 2022), increasing positive correlations between $\delta^{13}C$ and $\delta^{18}O$ values during the SW-CIE in all environmental categories may indicate the influence of ubiquitous in-situ and/or more immediate post depositional diagenetic effects (Fig. 4D). Increasingly positive correlations between $\delta^{13}C$ and $\delta^{18}O$ during the SW-CIE that then precipitously decrease during the recovery (Fig. 4D) could also be indicative of an increased flux of oceanic alkalinity (Spero et al., 1997) as a driver of increased carbonate deposition.

Although carbon cycling perturbation need not be mutually exclusive with existing hypotheses explaining the extreme magnitude of the SW-CIE, the results presented and discussed above suggest that explanations must also provide a mechanism for the coincident increase in carbonate quantity across depositional environments that had a dominantly dolostone phase (Figures 2, 3; Macdonald et al., 2023; Segessenman and Peters, 2023; Bowyer et al., 2024). The SW-CIE was coincident with the largest increase in dolostone quantity observed during the Ediacaran (post-cap carbonate), with subsequent carbonate quantity increases dominantly reported as limestone (Fig. 3). Until recently, this observation may have suggested diagenetic effects on SW-CIE carbonates due to the nature of the 'dolomite problem' in which there has been a long-standing challenge in understanding mechanisms of primary dolomite deposition (Land, 1998). Although there is still much to be understood about potential primary dolomite precipitation (Kim et al., 2023; Wang W. et al., 2023), it has recently been demonstrated that abiotic primary dolomite precipitation can occur when dissolved silica is present in high Mg:Ca ratio solutions at room temperature (Fang and Xu, 2022a; Fang and Xu,

2022b; Fang et al., 2023). Mid-Ediacaran bedded chert from North America has been reported in the Drook Fm (labeled as chemical sediments/evaporitic in Segessenman and Peters, 2023) of Newfoundland and coincides with the SW-CIE, a potential indicator of elevated dissolved silica in mid-Ediacaran oceans (Keppie et al., 1979; Williams and King, 1979; Segessenman and Peters, 2023). Furthermore, dissolved silica has been implicated as an influential factor for the soft-bodied Ediacaran biota's unique preservation within siliciclastic rocks (Tarhan et al., 2016; Slagter et al., 2021; Slagter et al., 2024), some of the oldest examples of which temporally overlap with the SW-CIE interval (Figs. 2-3; Table 2). This also coincides with increased Gondwana amalgamation orogenesis and felsic CIMP LIP emplacement (Aleinikoff et al. 1995; Southworth et al., 2009; Schmitt et al., 2018; Condie et al., 2021; Müller et al., 2024), a potential source for increased silica input to the mid-Ediacaran oceans (Figs. 2-5; Table 2). Siliciclastic weathering in a higher $pCO_2$ atmosphere can be a significant source of ocean alkalinity, a potential tie-in to the increased correlation between $\delta^{13}C$ and $\delta^{18}O$ during the SW-CIE (Fig. 4D; Halevy and Bachan, 2017; Middelburg et al., 2020) Considering these studies, the relative rarity of Ediacaran biota-style preservation in the Phanerozoic may be attributed to the radiation of biosilicifiers such as sponges and radiolarians drawing down oceanic dissolved silica during the early Cambrian (Conley et al., 2017; Ye et al., 2021). This may also help to explain the assumed (but still debated) decreased prevalence of dolomite through geologic time (Schomaker et al., 1985; Li et al., 2021; Husson and Coogan, 2023), potentially signifying Ediacaran dolomite quantity and Ediacaran biota preservation styles as additional factors that mark the Ediacaran as a critical transition period.

During the SW-CIE's 'recovery' interval to less negative $\delta^{13}C$ values, there is a sharp decrease in carbonate quantity that is immediately followed by another sharp carbonate quantity

586 increase (dominantly limestone) that is not associated with a $\delta^{13}C$ excursion, which coincides
587 with the timeframe of the proposed Luoquan glaciation (Figs. 2-5; Table 2). The bracketing of
588 the SW-CIE by glacially influenced strata, like that of the Trezona anomaly (Halverson et al.,
589 2020), may indicate that the SW-CIE took place during an interglacial warm/hot interval. The
590 mechanisms that could have driven this potential relative model of mid-Ediacaran events have
591 been laid out above: Gondwana amalgamation increases in orogenic belt length increased
592 weathering induced $CO_2$ drawdown, which may have eventually induced glaciation (in addition
593 to other factors that affect Earth's climate sensitivity, e.g., latitudinal distribution of continents)
594 associated with the Gaskiers. The Acraman impact event appears unlikely to have been an
595 initiator of the Gaskiers glaciation, as there is evidence of ice-rafted debris stratigraphically
596 above and below the Acraman's associated ejecta band (Gostin et al., 2010; Williams and
597 Schmidt, 2021). Depending on the extent of glaciation, ice coverage could have slowed the rate
598 of weathering related $CO_2$ drawdown, and when paired with coeval CIMP LIP outgassing, tipped
599 the climate threshold to a warm/hothouse state. During this warm interval, rates of weathering
600 would have accelerated (including of the emplaced Catoctin LIP, which consists of felsic
601 volcanics; Aleinikoff et al., 1999; Southworth et al., 2009) and delivered elevated rates of
602 elements such as sulfur, phosphorus, and silica to the mid-Ediacaran oceans, which may have
603 played an influential role in the SW-CIE, transient $O_2$ ventilation of the oceans, and the first
604 occurrences of the Ediacaran biota and their unique taphonomy (Figs. 2-5). A transition from
605 glaciation to a warm/hothouse state would have contributed to transgressive systems tracts
606 associated with the SW-CIE, and a return to glacial conditions after the SW-CIE could explain
607 the sharp decrease in carbonate quantity, although this could be caused by siliciclastic drowning
608 of carbonates at this time as well. The Luoquan glaciation that follows the SW-CIE interval may

represent the accelerated weathering drawdown of atmospheric $CO_2$ from continued Gondwana amalgamation and/or weathering of CIMP volcanics that initiated a return to cool/icehouse conditions, in a similar cycle as proposed for the Cryogenian return to Snowball Earth after Sturtian deglaciation (Hoffman and Schrag, 2002; Nance, 2022).

### 4.5 Carbonate environments, the Ediacaran biota, and the appearance of biomineralizers

Late Ediacaran glacially influenced strata, found outside of North America, although loosely constrained, are generally absent by ~550 Ma (Wang R. et al., 2023b; Wang R. et al., 2023c). Conspicuously, there is an increase in nearshore depositional environment carbonate quantity that is dominantly limestone from 550-545 Ma (Figs 2-3). There is an overall decreasing trend in $\delta^{13}C$ values that begins at ~552 Ma and both slope/basin and outer shelf categories exhibit averages that may be related to potential excursions at the end of the Ediacaran (Yang et al., 2021), though it is far less definitive than that of the SW-CIE (Fig. 4B-C). The increase in nearshore carbonate quantity is also coincident with final pulses of the CIMP/Laurentian rifting (Condie et al., 2021; Ernst et al., 2021) and the first occurrences of the oldest known biomineralizers (and presumed metazoans) such as *Cloudinia*, *Namacalathus*, or *Shaanxilithes* (Xiao and Narbonne, 2020; Shore et al., 2021; Wang et al., 2021). Interestingly, these latest Ediacaran biomineralizers are currently some of the oldest Ediacaran biota taxa to be found within carbonate lithologies, whereas most of the rest of the Ediacaran biota are found as molds within siliciclastic rocks (Xiao and Narbonne, 2020; Droser et al., 2022). We do not assert that expansion of nearshore carbonate environments directly drove the advent of metazoan biomineralization, but rather that the coincident change in depositional environment characteristics may have helped to shape circumstances in which biomineralization and

colonization of carbonate-rich shallow marine environments was advantageous. Tectonic and glacioeustatic driven sea level rise may have increased shallow marine habitable environments and/or non-carbonate dominated shallow marine settings may have become less hospitable due to redox changes, thus providing the impetus for biological adaptation and expansion into carbonate depositional environments (Evans et al., 2022; Caxito et al., 2024; Zhang et al., 2024).

More broadly, it is worth noting that biodiversity trends of the informal Ediacaran biota's Avalon, White Sea, and Nama divisions are broadly coincident with the environmental/climactic transitions presented and discussed thus far (Evans et al., 2022; Fig. 6 of Bowyer et al., 2024; Segessenman and Peters, 2024): 1) Avalon peak generic richness reaches maximum diversity coincident with the SW-CIE's recovery, but decreases sharply as carbonate quantity sharply decreases; 2) White Sea generic richness abruptly increases coincident with the second pulse of carbonate quantity and decreases/transitions to the Nama at the ~550 Ma end of the Luoquan glaciation; 3) Nama generic richness is never as high as that of the Avalon or White Sea, but its peak is nominally coincident with the final pulse of carbonate quantity during the latest Ediacaran; 4) The Ediacaran biota declines across the Ediacaran-Cambrian boundary, coincident with decreases in carbonate quantity, regression (Shahkarami et al., 2020), and the advent of Cambrian small shelly faunas (Bowyer et al., 2024). However, the Ediacaran biota has largely been found in non-carbonate lithologies and the Avalon assemblage is generally associated with deeper marine settings (Xiao and Narbonne, 2020), so we are not attributing a direct connection between carbonate depositional environment and Ediacaran biodiversity (at least not for the Avalon or White Sea assemblages). Increases in accommodation may have promoted greater burial of organic carbon within long-term reservoirs of continental margins, thus enabling atmospheric and/or oceanic oxygen buildup (e.g., Husson and Peters, 2017; Zhang et al., 2019;

Cao et al., 2020; Li et al., 2020; Shi et al., 2023), a potential necessity for evolutionary developments of the Ediacaran biota (Sperling et al., 2015; Evans et al., 2018; Evans et al., 2022). Ediacaran organisms themselves may have played a role in shaping environments to better suit them, with fluid dynamics analyses suggesting that early Ediacaran communities may have promoted ocean $O_2$ ventilation (Schiffbauer and Bykova, 2024) and increasing ecosystem engineering by putative metazoans in the late Ediacaran may have promoted macroevolutionary change across the Ediacaran-Cambrian boundary (Mussini and Dunn, 2024). However, it should be noted that redox proxies, physiology, and life habits of Ediacaran organisms are not straight-forward to interpret and are complex, challenging topics that are areas of ongoing development (e.g., Boag et al., 2018; Cherry et al., 2022; Gong et al., 2023; Mussini and Dunn, 2024). Despite the complexities, Ediacaran carbonate quantity and geochemistry may serve as proxies signifying common cause mechanisms known from the Phanerozoic of glacioeustacy, rifting, and supercontinent amalgamation that drove Ediacaran marine depositional environment changes, global climate shifts, and macroevolution.

While there are still many unknowns regarding the Ediacaran and age constraints, there is at least one more known factor that likely contributed to the evolution of Earth-systems dynamics in the Ediacaran and Cambrian Periods that should be included in considerations of the SW-CIE, global climate dynamics, and Ediacaran macroevolution. An identified ultra-low time-averaged field intensity (UL-TAFI) of Earth's magnetic field, potentially related to a late inner core nucleation and estimated to be 10-30 times weaker than in the modern, appears to reach a minimum in the middle Ediacaran and continues through to the middle Cambrian (Huang et al., 2024). This is a seemingly unique event in Earth history that overlaps with the SW-CIE, the Ediacaran biota's appearance, potential climactic shifts in the middle to late Ediacaran, and the

678 Cambrian radiation of metazoans (Bono et al., 2019; Li et al., 2023; Huang et al., 2024). The
679 UL-TAFI may have allowed for an increase in the rate of hydrogen stripping from the upper
680 atmosphere by solar wind. This in turn could have led to oxygenation of Earth's atmosphere,
681 perhaps contributing to the expression of the SW-CIE and the appearance of shallow marine taxa
682 from the Ediacaran biota (Urey, 1952; Siscoe and Chen, 1975; Meert et al., 2016; Huang et al.,
683 2024). This has also contributed to the difficulty of developing paleogeographic reconstructions
684 for the Ediacaran, a critical component to assessing the influences of various tectonics on global
685 climate and macroevolution (Domeier et al., 2023). As an emerging area of discussion and
686 research, it remains unclear how the UL-TAFI may have influenced other Earth systems in the
687 Ediacaran. If the UL-TAFI was related to a late-stage inner core nucleation (Bono et al., 2019; Li
688 et al., 2023), how might that have affected mantle convection dynamics that drove tectonic
689 events affecting shallow shelf area, carbonate quantity and geochemistry such as Laurentian
690 rifting, CIMP magmatism, and Gondwana's amalgamation? Could a severely weakened
691 magnetic field have contributed to shifts in global climate dynamics or influenced the
692 development of ozone? How might higher UV exposure in shallow marine environments have
693 shaped the evolution of the Ediacaran biota and early to middle Cambrian faunas? These are all
694 intriguing questions that have been posed (Meert et al., 2016; Pan and Li, 2023) and require
695 further exploration. Although the exact nature of the UL-TAFI's contribution is unknown, it
696 seems unlikely that it did not have any influence and is worth considering for hypotheses
697 concerning Earth systems evolution during the middle Ediacaran to middle Cambrian.
698

699 **5. Conclusions**

Continental scale tectonic mechanisms such as orogenic silicate weathering and LIP magmatism/weathering are mechanisms that have been tied to both cooling and warming of global climate in the Phanerozoic via the release and drawdown of $CO_2$, including Pangea amalgamation as a driver of the Late Paleozoic Ice Age and Himalayan mountain-building as a driver of Cenozoic glaciation (Condie et al., 2021; Youbi et al., 2021; Nance, 2022). However, other factors unique to each of these periods/events are also considered to be important contributors to how effective tectonics are in levering global climate. Are there other major components to the outgassing, such as elevated sulfate? What is the composition of emplaced LIPs and how quickly do they weather (these first two points are tied to initiation of Sturtian glaciation; e.g., Macdonald and Swanson-Hysell, 2023)? How close to the equator was $CO_2$ outgassing (also tied to the initiation of Cryogenian glaciation)? What is the composition of rock being weathered during orogenic events (e.g., Tonian evaporite weathering related to SW-CIE; Shields et al., 2019) or of LIP magmas that are emplaced and weathered? The biosphere has also played a major role in periods of major $CO_2$ drawdown (and $pO_2$ buildup), such as the burial of organic matter in widespread anoxic swamps in the Permo-Carboniferous (Kent and Muttoni, 2020). Some truly unique drivers have been proposed for the end-Ordovician glaciation in the form of an orbital debris ring caused by a near-Earth asteroid breakup shading the equator (Tomkins et al., 2024). The dynamic interplay of the global climate levers listed above highlights that although familiar drivers affect Earth's climate throughout its history, every period has unique dynamics that change the balance and sensitivity of feedback mechanisms contributing to Earth systems evolution. The Ediacaran appears to have been a unique global state of major continental rifting coeval with major orogenesis that potentially shaped global climate, depositional environments, and macroevolutionary trends of the oldest known metazoans, the

723 signals of which may be reflected in continental scale carbonate deposition quantity and
724 geochemistry.

725 Changes in the estimated quantities of the preserved carbonate record can be difficult to
726 interpret, as continental scale controls on deposition and preservation are often complex
727 combinations of multiple global and local scale controls in addition to potential post-deposition
728 deformation and erosion of strata that were preserved. However, by analyzing carbonate quantity
729 with regards to the unique geologic context of the Ediacaran and their depositional environments,
730 we found that patterns of North American carbonate deposition are largely consistent with
731 existing hypotheses of Ediacaran tectonic forcings that may have influenced long term sea level,
732 climate, marine redox states, and macroevolution. Additionally, a mid-Ediacaran carbonate
733 quantity maximum that is dominantly dolostone increases across all categories of depositional
734 environments and is coeval with the hallmark negative $\delta^{13}C$ values of the SW-CIE, which
735 supports the idea of a continental-scale transgressive event that was, at least in part, driven by
736 global tectonics and glacioeustacy. These findings indicate that the magnitude of the SW-CIE
737 excursion may have had at least some contribution from global carbon cycling perturbation and
738 that the uniquely extreme magnitude of the SW-CIE may be a mixed signal of oceanic DIC $\delta^{13}C$
739 and proposed mechanisms that could have decoupled shallow marine carbonate $\delta^{13}C$. The
740 Ediacaran biota's oldest known occurrences also coincide with the Ediacaran carbonate
741 maximum, and the first occurrences of Ediacaran biomineralizers coincide with the final pulse of
742 dominantly nearshore carbonate quantity, potentially supporting common cause drivers of
743 carbonate quantity and macroevolution during the mid-to-late Ediacaran. Ediacaran carbonate
744 quantity and geochemistry, when combined with results of studies compiling and establishing the
745 timings of potentially globally influential events (e.g., Gondwana amalgamation, CIMP

746 magmatism, and others discussed previously), may serve as a rough proxy for long-term climate
747 and tectonic dynamics that shaped the evolution of Earth's oldest complex macroscopic
748 organisms. While the results presented here are generally consistent with studies that include
749 global compilations of relevant key stratigraphic sections, the extent to which the aggregate
750 quantity and geochemistry of carbonates from the Ediacaran System of North America are
751 representative of the Ediacaran Earth remains unknown. Expansion of this dataset and the
752 analyses presented here to include other continents and geochemical data, continued
753 establishment of new geochronologic constraints, and further geochemical analysis of proxies
754 that enable reconstruction of Ediacaran paleoclimate will further enhance our understanding of
755 Earth systems evolution during the dawn of animal life.
756

757 **Acknowledgements**

758 DCS was supported in part by the Dean L. Morgridge graduate fellowship, the University of
759 Wisconsin-Madison Dept. of Geoscience, and the George Mason University Atmospheric,
760 Oceanic, and Earth Sciences Dept. We thank J. Husson and B. Hupp for feedback on early drafts
761 of this manuscript. We also thank G. Gilleaudeau and A.J. Kaufman for insightful feedback on
762 topics presented in this manuscript. Macrostrat infrastructure development was supported by US
763 National Science Foundation EAR-1150082 and EarthCube ICER-1440312.
764

765 **References**

766 Ahm, A.-S.C., Bjerrum, C.J., Hoffman, P.F., Macdonald, F.A., Maloof, A.C., Rose, C.V.,
767 Strauss, J.V., Higgins, J.A., 2021. The Ca and Mg isotope record of the Cryogenian

768 Trezona carbon isotope excursion. Earth and Planetary Science Letters 568, 117002.
769 https://doi.org/10.1016/j.epsl.2021.117002
770 Ahm, A.-S.C., Husson, J.M., 2022. Local and global controls on carbon isotope
771 chemostratigraphy: Cambridge University Press. https://doi.org/10.1017/9781009028882
772 Ahm, A.-S.C., Maloof, A.C., Macdonald, F.A., Hoffman, P.F., Bjerrum, C.J., Bold, U., Rose,
773 C.V., Strauss, J.V., Higgins, J.A., 2019. An early diagenetic deglacial origin for basal
774 Ediacaran "cap dolostones." Earth and Planetary Science Letters 506, 292–307.
775 https://doi.org/10.1016/j.epsl.2018.10.046
776 Alcott, L.J., Walton, C., Planavsky, N.J., Shorttle, O., Mills, B.J.W., 2024. Crustal carbonate
777 build-up as a driver for Earth's oxygenation. Nature Geoscience 17, 458–464.
778 https://doi.org/10.1038/s41561-024-01417-1
779 Aleinikoff, J.N., Zartman, R.E., Walter, M., Rankin, D.W., Lyttle, P.T., Burton, W.C., 1995. U-
780 Pb Ages of Metarhyolites of the Catoctin and Mount Rogers Formations, Central and
781 Southern Appalachians: Evidence for Two Pulses of Iapetan Rifting. American Journal of
782 Science 295, 428–454. https://doi.org/10.2475/ajs.295.4.428
783 Beranek, L.P., Hutter, A.D., Pearcey, S., James, C., Langor, V., Pike, C., Goudie, D., Oldham,
784 L., 2023. New evidence for the Baltican cratonic affinity and Tonian to Ediacaran
785 tectonic evolution of West Avalonia in the Avalon Peninsula, Newfoundland, Canada.
786 Precambrian Research 390, 107046. https://doi.org/10.1016/j.precamres.2023.107046
787 Bergmann, K.D., Zentmyer, R.A., Fischer, W.W., 2011. The stratigraphic expression of a large
788 negative carbon isotope excursion from the Ediacaran Johnnie Formation, Death Valley.
789 Precambrian Research 188, 45–56. https://doi.org/10.1016/j.precamres.2011.03.014

790 Boag, T.H., Stockey, R.G., Elder, L.E., Hull, P.M., Sperling, E.A., 2018. Oxygen, temperature
791 and the deep-marine stenothermal cradle of Ediacaran evolution. Proceedings of the
792 Royal Society B 285, 20181724. https://doi.org/10.1098/rspb.2018.1724
793 Bobrovskiy, I., Hope, J.M., Ivantsov, A., Nettersheim, B.J., Hallmann, C., Brocks, J.J., 2018.
794 Ancient steroids establish the Ediacaran fossil *Dickinsonia* as one of the earliest animals.
795 Science 361, 1246–1249. https://doi.org/10.1126/science.aat7228
796 Bono, R.K., Tarduno, J.A., Nimmo, F., Cottrell, R.D., 2019. Young inner core inferred from
797 Ediacaran ultra-low geomagnetic field intensity. Nature Geoscience 12, 143–147.
798 https://doi.org/10.1038/s41561-018-0288-0
799 Boulila, S., Peters, S.E., Müller, R.D., Haq, B.U., Hara, N., 2023. Earth's interior dynamics drive
800 marine fossil diversity cycles of tens of millions of years. Proceedings of the National
801 Academy of Sciences of the United States of America 120, e2221149120.
802 https://doi.org/10.1073/pnas.2221149120
803 Bowyer, F.T., Uahengo, C.-I., Kaputuaza, K., Ndeunyema, J., Yilales, M., Alexander, R.D.,
804 Curtis, A., Wood, R.A., 2023. Constraining the onset and environmental setting of
805 metazoan biomineralization: The Ediacaran Nama Group of the Tsaus Mountains,
806 Namibia. Earth and Planetary Science Letters 620, 118336.
807 https://doi.org/10.1016/j.epsl.2023.118336
808 Bowyer, F.T., Wood, R.A., Yilales, M., 2024. Sea level controls on Ediacaran-Cambrian animal
809 radiations. Sci. Adv. 10, eado6462. https://doi.org/10.1126/sciadv.ado6462
810 Bowyer, F.T., Zhuravlev, A.Y., Wood, R., Shields, G.A., Zhou, Y., Curtis, A., Poulton, S.W.,
811 Condon, D.J., Yang, C., Zhu, M., 2022. Calibrating the temporal and spatial dynamics of

812 the Ediacaran - Cambrian radiation of animals. Earth-Science Reviews 225, 103913.
813 https://doi.org/10.1016/j.earscirev.2021.103913
814 Brendan Murphy, J., Damian Nance, R., Johnston, S.T., Casas, J.M., Cawood, P.A., Matheson,
815 E.J., Pufahl, P.K., Dan, W., Javier Álvaro, J., Heron, P.J., Strachan, R.A., 2024.
816 Speculations on the Paleozoic legacy of Gondwana amalgamation. Gondwana Research
817 129, 107–131. https://doi.org/10.1016/j.gr.2023.12.002
818 Busch, J.F., Boag, T.H., Sperling, E.A., Rooney, A.D., Feng, X., Moynihan, D.P., Strauss, J.V.,
819 2023. Integrated Litho-, Chemo- and Sequence Stratigraphy of the Ediacaran Gametrail
820 Formation Across a Shelf-Slope Transect in the Wernecke Mountains, Yukon, Canada.
821 American Journal of Science 323. https://doi.org/10.2475/001c.74874
822 Busch, J.F., Hodgin, E.B., Ahm, A.-S.C., Husson, J.M., Macdonald, F.A., Bergmann, K.D.,
823 Higgins, J.A., Strauss, J.V., 2022. Global and local drivers of the Ediacaran Shuram
824 carbon isotope excursion. Earth and Planetary Science Letters 579, 117368.
825 https://doi.org/10.1016/j.epsl.2022.117368
826 Busch, J.F., Rooney, A.D., Meyer, E.E., Town, C.F., Moynihan, D.P., Strauss, J.V., 2021. Late
827 Neoproterozoic – early Paleozoic basin evolution in the Coal Creek inlier of Yukon,
828 Canada: implications for the tectonic evolution of northwestern Laurentia. Canadian
829 Journal of Earth Sciences 58, 355–377. https://doi.org/10.1139/cjes-2020-0132
830 Canfield, D.E., Knoll, A.H., Poulton, S.W., Narbonne, G.M., Dunning, G.R., 2020. Carbon
831 isotopes in clastic rocks and the Neoproterozoic carbon cycle. American Journal of
832 Science 320, 97–124. https://doi.org/10.2475/02.2020.01

833 Cantine, M.D., Knoll, A.H., Bergmann, K.D., 2020. Carbonates before skeletons: A database
834 approach. Earth-Science Reviews 201, 103065.
835 https://doi.org/10.1016/j.earscirev.2019.103065
836 Cantine, M.D., Rooney, A.D., Knoll, A.H., Gómez-Pérez, I., Al Baloushi, B., Bergmann, K.D.,
837 2024. Chronology of Ediacaran sedimentary and biogeochemical shifts along eastern
838 Gondwanan margins. Communications Earth & Environment 5, 520.
839 https://doi.org/10.1038/s43247-024-01630-1
840 Cao, M., Daines, S.J., Lenton, T.M., Cui, H., Algeo, T.J., Dahl, T.W., Shi, W., Chen, Z.-Q.,
841 Anbar, A., Zhou, Y.-Q., 2020. Comparison of Ediacaran platform and slope δ238U
842 records in South China: Implications for global-ocean oxygenation and the origin of the
843 Shuram Excursion. Geochimica et Cosmochimica Acta 287, 111–124.
844 https://doi.org/10.1016/j.gca.2020.04.035
845 Caxito, F., Lana, C., Frei, R., Uhlein, G.J., Sial, A.N., Dantas, E.L., Pinto, A.G., Campos, F.C.,
846 Galvão, P., Warren, L.V., Okubo, J., Ganade, C.E., 2021. Goldilocks at the dawn of
847 complex life: mountains might have damaged Ediacaran–Cambrian ecosystems and
848 prompted an early Cambrian greenhouse world. Scientific Reports 11, 20010.
849 https://doi.org/10.1038/s41598-021-99526-z
850 Caxito, F.A., Sperling, E., Fazio, G., Adorno, R.R., Denezine, M., Carmo, D.A.D., Giorgioni,
851 M., Uhlein, G.J., Sial, A.N., 2024. A shift in redox conditions near the
852 Ediacaran/Cambrian transition and its possible influence on early animal evolution,
853 Corumbá Group, Brazil. Geoscience Frontiers 15, 101810.
854 https://doi.org/10.1016/j.gsf.2024.101810

855 Cherry, L.B., Gilleaudeau, G.J., Grazhdankin, D.V., Romaniello, S.J., Martin, A.J., Kaufman,
856 A.J., 2022. A diverse Ediacara assemblage survived under low-oxygen conditions. Nature
857 Communications 13, 7306. https://doi.org/10.1038/s41467-022-35012-y
858 Cochrane, D.J.W., Navarro, L., Arnott, R.W.C., 2019. Sedimentological and geochemical
859 evolution of an Ediacaran mixed carbonate-siliciclastic continental slope system,
860 Windermere Supergroup, southern Canadian Cordillera, British Columbia, Canada.
861 Precambrian Research 327, 47–67. https://doi.org/10.1016/j.precamres.2019.02.021
862 Condie, K.C., Pisarevsky, S.A., Puetz, S.J., 2021. LIPs, orogens and supercontinents: The
863 ongoing saga. Gondwana Research 96, 105–121. https://doi.org/10.1016/j.gr.2021.05.002
864 Conley, D.J., Carey, J.C., 2015. Silica cycling over geologic time. Nature Geoscience 8, 431–
865 432. https://doi.org/10.1038/ngeo2454
866 Conley, D.J., Frings, P.J., Fontorbe, G., Clymans, W., Stadmark, J., Hendry, K.R., Marron, A.O.,
867 De La Rocha, C.L., 2017. Biosilicification Drives a Decline of Dissolved Si in the
868 Oceans through Geologic Time. Frontiers in Marine Science 4, 397.
869 https://doi.org/10.3389/fmars.2017.00397
870 Corsetti, F.A., Hagadorn, J.W., 2000. Precambrian-Cambrian transition: Death Valley, United
871 States. Geology 28, 299–302. https://doi.org/10.1130/0091-
872 7613(2000)28<299:PTDVUS>2.0.CO;2
873 Corsetti, F.A., J. Kaufman, A.J., 2003. Stratigraphic investigations of carbon isotope anomalies
874 and Neoproterozoic ice ages in Death Valley, California. Geological Society of America
875 Bulletin 115, 916–932. https://doi.org/10.1130/B25066.1
876 Corsetti, F.A., Kaufman, A.J., 1994. Chemostratigraphy of Neoproterozoic-Cambrian Units,
877 White-Inyo Region, Eastern California and Western Nevada: Implications for Global

878 Correlation and Faunal Distribution. PALAIOS 9, 211–219.
879 https://doi.org/10.2307/3515107
880 Cramer, B.D., Jarvis, I., 2020. Carbon Isotope Stratigraphy, in: Gradstein, F.M., Ogg, J.G.,
881 Schmitz, M.D., Ogg, G.M. (Eds.), Geologic Time Scale 2020. Elsevier, pp. 309–343.
882 https://doi.org/10.1016/B978-0-12-824360-2.00011-5
883 Creveling, J.R., Bergmann, K.D., Grotzinger, J.P., 2016. Cap carbonate platform facies model,
884 Noonday Formation, SE California. Geological Society of America Bulletin 128, 1249–
885 1269. https://doi.org/10.1130/B31442.1
886 Creveling, J.R., Mitrovica, J.X., 2014. The sea-level fingerprint of a Snowball Earth
887 deglaciation. Earth and Planetary Science Letters 399, 74–85.
888 https://doi.org/10.1016/j.epsl.2014.04.029
889 Cui, H., Kaufman, A.J., Xiao, S., Zhou, C., Liu, X.-M., 2017. Was the Ediacaran Shuram
890 Excursion a globally synchronized early diagenetic event? Insights from methane-derived
891 authigenic carbonates in the uppermost Doushantuo Formation, South China. Chemical
892 Geology 450, 59–80. https://doi.org/10.1016/j.chemgeo.2016.12.010
893 Cui, H., Kaufman, A.J., Xiao, S., Zhou, C., Zhu, M., Cao, M., Loyd, S., Crockford, P., Liu, X.-
894 M., Goderis, S., Wang, W., Guan, C., 2022. Dynamic interplay of biogeochemical C, S
895 and Ba cycles in response to the Shuram oxygenation event. Journal of the Geological
896 Society of London 179, jgs2021-081. https://doi.org/10.1144/jgs2021-081
897 Cui, H., Kitajima, K., Orland, I.J., Xiao, S., Baele, J.-M., Kaufman, A.J., Denny, A., Zhou, C.,
898 Spicuzza, M.J., Fournelle, J.H., Valley, J.W., 2021. Deposition or diagenesis? Probing
899 the Ediacaran Shuram excursion in South China by SIMS. Global and Planetary Change
900 206, 103591. https://doi.org/10.1016/j.gloplacha.2021.103591

Darroch, S.A.F., Cribb, A.T., Buatois, L.A., Germs, G.J.B., Kenchington, C.G., Smith, E.F., Mocke, H., O'Neil, G.R., Schiffbauer, J.D., Maloney, K.M., Racicot, R.A., Turk, K.A., Gibson, B.M., Almond, J., Koester, B., Boag, T.H., Tweedt, S.M., Laflamme, M., 2021. The trace fossil record of the Nama Group, Namibia: Exploring the terminal Ediacaran roots of the Cambrian explosion. Earth-Science Reviews 212, 103435. https://doi.org/10.1016/j.earscirev.2020.103435

Derry, L.A., 2010. A burial diagenesis origin for the Ediacaran Shuram–Wonoka carbon isotope anomaly. Earth and Planetary Science Letters 294, 152–162. https://doi.org/10.1016/j.epsl.2010.03.022

Dewey, J., Spall, H., 1975. Pre-Mesozoic plate tectonics: How far back in Earth history can the Wilson Cycle be extended? Geology 3, 422–424. https://doi.org/10.1130/0091-7613(1975)3<422:PPTHFB>2.0.CO;2

Dodd, M.S., Shi, W., Li, C., Zhang, Z., Cheng, M., Gu, H., Hardisty, D.S., Loyd, S.J., Wallace, M.W., vS. Hood, A., Lamothe, K., Mills, B.J.W., Poulton, S.W., Lyons, T.W., 2023. Uncovering the Ediacaran phosphorus cycle. Nature 618, 974–980. https://doi.org/10.1038/s41586-023-06077-6

Domeier, M., Robert, B., Meert, J.G., Kulakov, E.V., McCausland, P.J.A., Trindade, R.I.F., Torsvik, T.H., 2023. The enduring Ediacaran paleomagnetic enigma. Earth-Science Reviews 242, 104444. https://doi.org/10.1016/j.earscirev.2023.104444

Droser, M.L., Evans, S.D., Tarhan, L.G., Surprenant, R.L., Hughes, I.V., Hughes, E.B., Gehling, J.G., 2022. What Happens Between Depositional Events, Stays Between Depositional Events: The Significance of Organic Mat Surfaces in the Capture of Ediacara

923 Communities and the Sedimentary Rocks That Preserve Them. Frontiers in Earth Science
924 10, 826353. https://doi.org/10.3389/feart.2022.826353
925 Ernst, R.E., Bond, D.P.G., Zhang, S., Buchan, K.L., Grasby, S.E., Youbi, N., El Bilali, H.,
926 Bekker, A., Doucet, L.S., 2021. Large Igneous Province Record Through Time and
927 Implications for Secular Environmental Changes and Geological Time-Scale Boundaries,
928 in: Ernst, R.E., Dickson, A.J., Bekker, A. (Eds.), Geophysical Monograph Series. Wiley,
929 pp. 1–26. https://doi.org/10.1002/9781119507444.ch1
930 Evans, S.D., Diamond, C.W., Droser, M.L., Lyons, T.W., 2018. Dynamic oxygen and coupled
931 biological and ecological innovation during the second wave of the Ediacara Biota.
932 Emerging Topics in Life Sciences 2, 223–233. https://doi.org/10.1042/ETLS20170148
933 Evans, S.D., Tu, C., Rizzo, A., Surprenant, R.L., Boan, P.C., McCandless, H., Marshall, N.,
934 Xiao, S., Droser, M.L., 2022. Environmental drivers of the first major animal extinction
935 across the Ediacaran White Sea-Nama transition. Proceedings of the National Academy
936 of Sciences of the United States of America 119, e2207475119.
937 https://doi.org/10.1073/pnas.2207475119
938 Eyster, A., Ferri, F., Schmitz, M.D., Macdonald, F.A., 2018. One diamictite and two rifts:
939 Stratigraphy and geochronology of the Gataga Mountain of northern British Columbia.
940 American Journal of Science 318, 167–207. https://doi.org/10.2475/02.2018.1
941 Faehnrich, K., McClelland, W.C., Webb, L., Kośmińska, K., Strauss, J.V., 2023. Late
942 Ediacaran–early Cambrian rifting along the northern margin of Laurentia: constraints
943 from the Yelverton Formation of Ellesmere Island, Canada. Canadian Journal of Earth
944 Sciences 60, 1597–1626. https://doi.org/10.1139/cjes-2023-0020

945 Fairchild, I., Hambrey, M., 1995. Vendian basin evolution in East Greenland and NE Svalbard.
946 Precambrian Research 73, 217–233. https://doi.org/10.1016/0301-9268(94)00079-7
947 Fan, H., Chen, Z., Zhang, F., Zhu, C., Du, S., Zhang, Y., Wen, H., Khan, D., Algeo, T.J., 2025.
948 Seawater temperatures during the early to middle Ediacaran: Phosphate oxygen isotope
949 records. Chemical Geology 678, 122642. https://doi.org/10.1016/j.chemgeo.2025.122642
950 Fang, Y., Hobbs, F., Yang, Y., Xu, H., 2023. Dissolved silica-driven dolomite precipitation in
951 the Great Salt Lake, Utah, and its implication for dolomite formation environments.
952 Sedimentology 70, 1328–1347. https://doi.org/10.1111/sed.13081
953 Fang, Y., Xu, H., 2022a. Dissolved silica-catalyzed disordered dolomite precipitation. American
954 Mineralogist 107, 443–452. https://doi.org/10.2138/am-2021-7474
955 Fang, Y., Xu, H., 2022b. Coupled dolomite and silica precipitation from continental weathering
956 during deglaciation of the Marinoan Snowball Earth. Precambrian Research 380, 106824.
957 https://doi.org/10.1016/j.precamres.2022.106824
958 Fitzgerald, D.M., Narbonne, G.M., Pufahl, P.K., Dalrymple, R.W., 2024. The Mall Bay
959 Formation (Ediacaran) and the protracted onset of the Gaskiers glaciation in
960 Newfoundland, Canada. Precambrian Research 405, 107369.
961 https://doi.org/10.1016/j.precamres.2024.107369
962 Ganade De Araujo, C.E., Rubatto, D., Hermann, J., Cordani, U.G., Caby, R., Basei, M.A.S.,
963 2014. Ediacaran 2,500-km-long synchronous deep continental subduction in the West
964 Gondwana Orogen. Nature Communications 5, 5198.
965 https://doi.org/10.1038/ncomms6198

966 Gong, Z., Li, M., 2020. Astrochronology of the Ediacaran Shuram carbon isotope excursion,
967 Oman. Earth and Planetary Science Letters 547, 116462.
968 https://doi.org/10.1016/j.epsl.2020.116462
969 Gong, Z., Wei, G., Fakhraee, M., Alcott, L.J., Jiang, L., Zhao, M., Planavsky, N.J., 2023.
970 Revisiting marine redox conditions during the Ediacaran Shuram carbon isotope
971 excursion. Geobiology 21, 407–420. https://doi.org/10.1111/gbi.12547
972 Gostin, V.A., McKirdy, D.M., Webster, L.J., Williams, G.E., 2010. Ediacaran ice-rafting and
973 coeval asteroid impact, South Australia: insights into the terminal Proterozoic
974 environment. Australian Journal of Earth Sciences 57, 859–869.
975 https://doi.org/10.1080/08120099.2010.509408
976 Green, T., Renne, P.R., Keller, C.B., 2022. Continental flood basalts drive Phanerozoic
977 extinctions. Proceedings of the National Academy of Sciences of the United States of
978 America 119, e2120441119. https://doi.org/10.1073/pnas.2120441119
979 Grossman, E.L., Joachimski, M.M., 2020. Oxygen Isotope Stratigraphy, in: Gradstein, F.M.,
980 Ogg, J.G., Schmitz, M.D., Ogg, G.M. (Eds.), Geologic Time Scale 2020. Elsevier, pp.
981 279–307. https://doi.org/10.1016/B978-0-12-824360-2.00010-3
982 Grotzinger, J.P., Fike, D.A., Fischer, W.W., 2011. Enigmatic origin of the largest-known carbon
983 isotope excursion in Earth's history. Nature Geoscience 4, 285–292.
984 https://doi.org/10.1038/ngeo1138
985 Gu, H., Hu, J., Cheng, M., Wang, H., Dodd, M.S., Zhang, Z., Algeo, T.J., Li, C., 2024.
986 Heterogeneous coupling of δ13Corg and δ13Ccarb during the Shuram Excursion:
987 Implications for a large dissolved organic carbon reservoir in the Ediacaran ocean. Global
988 and Planetary Change 239, 104466. https://doi.org/10.1016/j.gloplacha.2024.104466

989 Hagadorn, J.W., Waggoner, B., 2000. Ediacaran Fossils from the southwestern Great Basin,
990 United States. Journal of Paleontology 74, 349-359. https://doi.org/10.1666/0022-
991 3360(2000)074<0349:EFFTSG>2.0.CO;2
992 Hagen, C.J., Creveling, J.R., 2024. An algorithm-guided Ediacaran global composite δ13Ccarb–
993 Bayesian age model. Palaeogeography, Palaeoclimatology, Palaeoecology 650, 112321.
994 https://doi.org/10.1016/j.palaeo.2024.112321
995 Halevy, I., Bachan, A., 2017. The geologic history of seawater pH. Science 355, 1069–1071.
996 https://doi.org/10.1126/science.aal4151
997 Halverson, G., Porter, S., Shields, G., 2020. The Tonian and Cryogenian Periods, in: Gradstein,
998 F.M., Ogg, J.G., Schmitz, M.D., Ogg, G.M. (Eds.), Geologic Time Scale 2020. Elsevier,
999 pp. 495–519. https://doi.org/10.1016/B978-0-12-824360-2.00017-6
1000 Halverson, G.P., Hoffman, P.F., Schrag, D.P., Maloof, A.C., Rice, A.H.N., 2005. Toward a
1001 Neoproterozoic composite carbon-isotope record. Geological Society of America Bulletin
1002 117, 1181. https://doi.org/10.1130/B25630.1
1003 Halverson, G.P., Maloof, A.C., Hoffman, P.F., 2004. The Marinoan glaciation (Neoproterozoic)
1004 in northeast Svalbard. Basin Research 16, 297–324. https://doi.org/10.1111/j.1365-
1005 2117.2004.00234.x
1006 Hannisdal, B., Peters, S.E., 2011. Phanerozoic Earth System Evolution and Marine Biodiversity.
1007 Science 334, 1121–1124. https://doi.org/10.1126/science.1210695
1008 Hatcher, R.D., 2010. The Appalachian orogen: A brief summary, in: Tollo, R.P., Bartholomew,
1009 M.J., Hibbard, J.P., Karabinos, P.M. (Eds.), From Rodinia to Pangea: The Lithotectonic
1010 Record of the Appalachian Region. Geological Society of America Memoirs 206, 1–19.
1011 https://doi.org/10.1130/2010.1206(01)

1012 Hebert, C.L., Kaufman, A.J., Penniston-Dorland, S.C., Martin, A.J., 2010. Radiometric and
1013 stratigraphic constraints on terminal Ediacaran (post-Gaskiers) glaciation and metazoan
1014 evolution. Precambrian Research 182, 402–412.
1015 https://doi.org/10.1016/j.precamres.2010.07.008
1016 Hodgin, E.B., Nelson, L.L., Wall, C.J., Barrón-Díaz, A.J., Webb, L.C., Schmitz, M.D., Fike,
1017 D.A., Hagadorn, J.W., Smith, E.F., 2021. A link between rift-related volcanism and end-
1018 Ediacaran extinction? Integrated chemostratigraphy, biostratigraphy, and U-Pb
1019 geochronology from Sonora, Mexico. Geology 49, 115–119.
1020 https://doi.org/10.1130/G47972.1
1021 Hoffman, P.F., 2011. Strange bedfellows: glacial diamictite and cap carbonate from the
1022 Marinoan (635 Ma) glaciation in Namibia. Sedimentology 58, 57–119.
1023 https://doi.org/10.1111/j.1365-3091.2010.01206.x
1024 Hoffman, P.F., Halverson, G.P., Domack, E.W., Maloof, A.C., Swanson-Hysell, N.L., Cox,
1025 G.M., 2012. Cryogenian glaciations on the southern tropical paleomargin of Laurentia
1026 (NE Svalbard and East Greenland), and a primary origin for the upper Russøya (Islay)
1027 carbon isotope excursion. Precambrian Research 206–207, 137–158.
1028 https://doi.org/10.1016/j.precamres.2012.02.018
1029 Hoffman, P.F., Kaufman, A.J., Halverson, G.P., Schrag, D.P., 1998. A Neoproterozoic Snowball
1030 Earth. Science 281, 1342–1346. https://doi.org/10.1126/science.281.5381.1342
1031 Hoffman, P.F., Li, Z.-X., 2009. A palaeogeographic context for Neoproterozoic glaciation.
1032 Palaeogeography, Palaeoclimatology, Palaeoecology 277, 158–172.
1033 https://doi.org/10.1016/j.palaeo.2009.03.013

1034 Hoffman, P.F., Schrag, D.P., 2002. The snowball Earth hypothesis: testing the limits of global
1035 change. Terra Nova 14, 129–155. https://doi.org/10.1046/j.1365-3121.2002.00408.x
1036 Hohmann, N., Koelewijn, J.R., Burgess, P., Jarochowska, E., 2024. Identification of the mode of
1037 evolution in incomplete carbonate successions. BMC Ecology and Evolution 24, 113.
1038 https://doi.org/10.1186/s12862-024-02287-2
1039 Huang, W., Tarduno, J.A., Zhou, T., Ibañez-Mejia, M., Dal Olmo-Barbosa, L., Koester, E.,
1040 Blackman, E.G., Smirnov, A.V., Ahrendt, G., Cottrell, R.D., Kodama, K.P., Bono, R.K.,
1041 Sibeck, D.G., Li, Y.-X., Nimmo, F., Xiao, S., Watkeys, M.K., 2024. Near-collapse of the
1042 geomagnetic field may have contributed to atmospheric oxygenation and animal radiation
1043 in the Ediacaran Period. Nature Communications Earth & Environment 5, 207.
1044 https://doi.org/10.1038/s43247-024-01360-4
1045 Husson, J.M., Coogan, L.A., 2023. River chemistry reveals a large decrease in dolomite
1046 abundance across the Phanerozoic. Geochemical Perspectives Letters 26, 1–6.
1047 https://doi.org/10.7185/geochemlet.2316
1048 Husson, J.M., Linzmeier, B.J., Kitajima, K., Ishida, A., Maloof, A.C., Schoene, B., Peters, S.E.,
1049 Valley, J.W., 2020. Large isotopic variability at the micron-scale in 'Shuram' excursion
1050 carbonates from South Australia. Earth and Planetary Science Letters 538, 116211.
1051 https://doi.org/10.1016/j.epsl.2020.116211
1052 Husson, J.M., Peters, S.E., 2017. Atmospheric oxygenation driven by unsteady growth of the
1053 continental sedimentary reservoir. Earth and Planetary Science Letters 460, 68–75.
1054 https://doi.org/10.1016/j.epsl.2016.12.012

1055 Ineson, J.R., Peel, J.S., Willman, S., Rugen, E.J., Sønderholm, M., Frykman, P., 2024.
1056 Lithostratigraphy of the Portfjeld Group (Ediacaran – lowermost Cambrian) of North
1057 Greenland. GEUS Bulletin 57. https://doi.org/10.34194/geusb.v57.8375
1058 Isson, T.T., Planavsky, N.J., 2018. Reverse weathering as a long-term stabilizer of marine pH
1059 and planetary climate. Nature 560, 471–475. https://doi.org/10.1038/s41586-018-0408-4
1060 Isson, T.T., Planavsky, N.J., Coogan, L.A., Stewart, E.M., Ague, J.J., Bolton, E.W., Zhang, S.,
1061 McKenzie, N.R., Kump, L.R., 2020. Evolution of the Global Carbon Cycle and Climate
1062 Regulation on Earth. Global Biogeochemical Cycles 34, e2018GB006061.
1063 https://doi.org/10.1029/2018GB006061
1064 Judd, E.J., Tierney, J.E., Lunt, D.J., Montañez, I.P., Huber, B.T., Wing, S.L., Valdes, P.J., 2024.
1065 A 485-million-year history of Earth's surface temperature. Science 385, eadk3705.
1066 https://doi.org/10.1126/science.adk3705
1067 Kendall, B.S., Creaser, R.A., Ross, G.M., Selby, D., 2004. Constraints on the timing of Marinoan
1068 "Snowball Earth" glaciation by 187Re–187Os dating of a Neoproterozoic, post-glacial
1069 black shale in Western Canada. Earth and Planetary Science Letters 222, 729–740.
1070 https://doi.org/10.1016/j.epsl.2004.04.004
1071 Kent, D.V., Muttoni, G., 2020. Pangea B and the Late Paleozoic Ice Age. Palaeogeography,
1072 Palaeoclimatology, Palaeoecology 553, 109753.
1073 https://doi.org/10.1016/j.palaeo.2020.109753
1074 Keppie, J.D., Dostal, J., Murphy, J.B., 1979. Petrology of the Late Precambrian Fourchu Group
1075 in the Louisbourg Area, Cape Breton Island: Nova Scotia Department of Mines and
1076 Energy 79-1, 18 p.

1077 Keppie, J.D., Keppie, D.F., 2024. Review and tectonic interpretation of Precambrian Avalonia.
1078 Geological Society of London Special Publications 542, 149–165.
1079 https://doi.org/10.1144/SP542-2022-356
1080 Kim, J., Kimura, Y., Puchala, B., Yamazaki, T., Becker, U., Sun, W., 2023. Dissolution enables
1081 dolomite crystal growth near ambient conditions. Science 382, 915–920.
1082 https://doi.org/10.1126/science.adi3690
1083 Kirschvink, J.L., 2023. A movable beast: glaciation in the Ediacaran. National Science Review
1084 10, nwad153. https://doi.org/10.1093/nsr/nwad153
1085 Knoll, A.H., Walter, M.R., Narbonne, G.M., Christie-Blick, N., 2006. The Ediacaran Period: a
1086 new addition to the geologic time scale. Lethaia 39, 13–30.
1087 https://doi.org/10.1080/00241160500409223
1088 Kump, L.R., Arthur, M.A., 1999. Interpreting carbon-isotope excursions: carbonates and organic
1089 matter. Chemical Geology 161, 181–198. https://doi.org/10.1016/S0009-2541(99)00086-
1090 8
1091 Laakso, T.A., Schrag, D.P., 2020. The role of authigenic carbonate in Neoproterozoic carbon
1092 isotope excursions. Earth and Planetary Science Letters 549, 116534.
1093 https://doi.org/10.1016/j.epsl.2020.116534
1094 Land, L.S., 1980. The Isotopic and Trace Element Geochemistry of Dolomite: The State of the
1095 Art, in: Zenger, D.H., Dunham, J.B., Ethington, R.L. (Eds.), Concepts and Models of
1096 Dolomitization. SEPM (Society for Sedimentary Geology).
1097 https://doi.org/10.2110/pec.80.28

1098 Land, L.S., 1998. Failure to Precipitate Dolomite at 25 °C from Dilute Solution Despite 1000-
1099 Fold Oversaturation after 32 Years. Aquatic Geochemistry 4, 361-368.
1100 https://doi.org/10.1023/A:1009688315854
1101 Lee, C., Love, G.D., Fischer, W.W., Grotzinger, J.P., Halverson, G.P., 2015. Marine organic
1102 matter cycling during the Ediacaran Shuram excursion. Geology G37236.1.
1103 https://doi.org/10.1130/G37236.1
1104 Li, M., Wignall, P.B., Dai, X., Hu, M., Song, H., 2021. Phanerozoic variation in dolomite
1105 abundance linked to oceanic anoxia. Geology 49, 698–702.
1106 https://doi.org/10.1130/G48502.1
1107 Li, R., Zhou, X., Eddy, M.P., Ickert, R.B., Wang, Z., Tang, D., Huang, K.-J., Peng, P., 2024.
1108 Stratigraphic evidence for a major unconformity within the Ediacaran System. Earth and
1109 Planetary Science Letters 636, 118715. https://doi.org/10.1016/j.epsl.2024.118715
1110 Li, Y.-X., Tarduno, J.A., Jiao, W., Liu, X., Peng, S., Xu, S., Yang, A., Yang, Z., 2023. Late
1111 Cambrian geomagnetic instability after the onset of inner core nucleation. Nature
1112 Communications 14, 4596. https://doi.org/10.1038/s41467-023-40309-7
1113 Li, Z., Cao, M., Loyd, S.J., Algeo, T.J., Zhao, H., Wang, X., Zhao, L., Chen, Z.-Q., 2020.
1114 Transient and stepwise ocean oxygenation during the late Ediacaran Shuram Excursion:
1115 Insights from carbonate δ238U of northwestern Mexico. Precambrian Research 344,
1116 105741. https://doi.org/10.1016/j.precamres.2020.105741
1117 Loyd, S.J., Marenco, P.J., Hagadorn, J.W., Lyons, T.W., Kaufman, A.J., Sour-Tovar, F.,
1118 Corsetti, F.A., 2012. Sustained low marine sulfate concentrations from the
1119 Neoproterozoic to the Cambrian: Insights from carbonates of northwestern Mexico and

eastern California. Earth and Planetary Science Letters 339–340, 79–94. https://doi.org/10.1016/j.epsl.2012.05.032

Ma, B., Tian, W., Wu, G., Nance, R.D., Zhao, Y., Chen, Y., Huang, S., 2022. The subduction-related Great Unconformity in the Tarim intracraton, NW China. Global and Planetary Change 215, 103883. https://doi.org/10.1016/j.gloplacha.2022.103883

Ma, C., Hames, W.E., Foster, D.A., Xiao, W., Mueller, P.A., Steltenpohl, M.G., 2023. Transformation of eastern North America from compression to extension in the Permian–Triassic, in: Whitmeyer, S.J., Williams, M.L., Kellett, D.A., Tikoff, B. (Eds.), Laurentia: Turning Points in the Evolution of a Continent. Geological Society of America, pp. 577–592. https://doi.org/10.1130/2022.1220(28)

Macdonald, F.A., McClelland, W.C., Schrag, D.P., Macdonald, W.P., 2009. Neoproterozoic glaciation on a carbonate platform margin in Arctic Alaska and the origin of the North Slope subterrane. Geological Society of America Bulletin 121, 448–473. https://doi.org/10.1130/B26401.1

Macdonald, F.A., Strauss, J.V., Sperling, E.A., Halverson, G.P., Narbonne, G.M., Johnston, D.T., Kunzmann, M., Schrag, D.P., Higgins, J.A., 2013. The stratigraphic relationship between the Shuram carbon isotope excursion, the oxygenation of Neoproterozoic oceans, and the first appearance of the Ediacara biota and bilaterian trace fossils in northwestern Canada. Chemical Geology 362, 250–272. https://doi.org/10.1016/j.chemgeo.2013.05.032

Macdonald, F.A., Swanson-Hysell, N.L., 2023. The Franklin Large Igneous Province and Snowball Earth Initiation. Elements 19, 296–301. https://doi.org/10.2138/gselements.19.5.296

1143 Macdonald, F.A., Yonkee, W.A., Flowers, R.M., Swanson-Hysell, N.L., 2023. Neoproterozoic
1144 of Laurentia, in: Laurentia: Whitmeyer, S.J., Williams, M.L., Kellett, D.A., Tikoff, B.
1145 (Eds.), Turning Points in the Evolution of a Continent. Geological Society of America,
1146 pp. 331–380. https://doi.org/10.1130/2022.1220(19)
1147 MacLennan, S.A., Eddy, M.P., Merschat, A.J., Mehra, A.K., Crockford, P.W., Maloof, A.C.,
1148 Southworth, C.S., Schoene, B., 2020. Geologic evidence for an icehouse Earth before the
1149 Sturtian global glaciation. Science Advances 6, eaay6647.
1150 https://doi.org/10.1126/sciadv.aay6647
1151 McDannell, K.T., Keller, C.B., Guenthner, W.R., Zeitler, P.K., Shuster, D.L., 2022.
1152 Thermochronologic constraints on the origin of the Great Unconformity. Proceedings of
1153 the National Academy of Sciences of the United States of America 119, e2118682119.
1154 https://doi.org/10.1073/pnas.2118682119
1155 McGee, B., Collins, A.S., Trindade, R.I.F., 2013. A Glacially Incised Canyon in Brazil: Further
1156 Evidence for Mid-Ediacaran Glaciation? The Journal of Geology 121, 275–287.
1157 https://doi.org/10.1086/669979
1158 Meert, J.G., Levashova, N.M., Bazhenov, M.L., Landing, E., 2016. Rapid changes of magnetic
1159 Field polarity in the late Ediacaran: Linking the Cambrian evolutionary radiation and
1160 increased UV-B radiation. Gondwana Research 34, 149–157.
1161 https://doi.org/10.1016/j.gr.2016.01.001
1162 Meert, J.G., Lieberman, B.S., 2008. The Neoproterozoic assembly of Gondwana and its
1163 relationship to the Ediacaran–Cambrian radiation. Gondwana Research 14, 5–21.
1164 https://doi.org/10.1016/j.gr.2007.06.007

1165 Meyers, S.R., Peters, S.E., 2011. A 56million year rhythm in North American sedimentation
1166 during the Phanerozoic. Earth and Planetary Science Letters 303, 174–180.
1167 https://doi.org/10.1016/j.epsl.2010.12.044
1168 Miall, A.D., 2016. The valuation of unconformities. Earth-Science Reviews 163, 22–71.
1169 https://doi.org/10.1016/j.earscirev.2016.09.011
1170 Middelburg, J.J., Soetaert, K., Hagens, M., 2020. Ocean Alkalinity, Buffering and
1171 Biogeochemical Processes. Reviews of Geophysics 58, e2019RG000681.
1172 https://doi.org/10.1029/2019RG000681
1173 Moynihan, D.P., Strauss, J.V., Nelson, L.L., Padget, C.D., 2019. Upper Windermere Supergroup
1174 and the transition from rifting to continent-margin sedimentation, Nadaleen River area,
1175 northern Canadian Cordillera. Geological Society of America Bulletin 131, 1673–1701.
1176 https://doi.org/10.1130/B32039.1
1177 Müller, R.D., Dutkiewicz, A., Zahirovic, S., Merdith, A.S., Scotese, C.R., Mills, B.J.W., Ilano,
1178 L., Mather, B., 2024. Solid Earth Carbon Degassing and Sequestration Since 1 Billion
1179 Years Ago. Geochemistry, Geophysics, Geosystems 25, e2024GC011713.
1180 https://doi.org/10.1029/2024GC011713
1181 Murphy, J.B., Nance, R.D., Wu, L., 2023. The provenance of Avalonia and its tectonic
1182 implications: a critical reappraisal. Geological Society of London Speical Publications
1183 531, 207–247. https://doi.org/10.1144/SP531-2022-176
1184 Mussini, G., Dunn, F.S., 2024. Decline and fall of the Ediacarans: late-Neoproterozoic
1185 extinctions and the rise of the modern biosphere. Biological Reviews 99, 110–130.
1186 https://doi.org/10.1111/brv.13014

1187 Myrow, P.M., Kaufman, A.J., 1999. A newly discovered cap carbonate above Varanger-Age
1188 glacial deposits in Newfoundland, Canada. Journal of Sedimentary Research 69, 784–
1189 793. https://doi.org/10.2110/jsr.69.784
1190 Myrow, P.M., Lamb, M.P., Ewing, R.C., 2018. Rapid sea level rise in the aftermath of a
1191 Neoproterozoic snowball Earth. Science 360, 649–651.
1192 https://doi.org/10.1126/science.aap8612
1193 Nance, R.D., 2022. The supercontinent cycle and Earth's long-term climate. Annals of the New
1194 York Academy of Sciences 1515, 33–49. https://doi.org/10.1111/nyas.14849
1195 Oriolo, S., Oyhantçabal, P., Wemmer, K., Siegesmund, S., 2017. Contemporaneous assembly of
1196 Western Gondwana and final Rodinia break-up: Implications for the supercontinent
1197 cycle. Geoscience Frontiers 8, 1431–1445. https://doi.org/10.1016/j.gsf.2017.01.009
1198 Pan, Y., Li, J., 2023. On the biospheric effects of geomagnetic reversals. National Science
1199 Review 10, nwad070. https://doi.org/10.1093/nsr/nwad070
1200 Peng, S.C., Babcock, L.E., Ahlberg, P., 2020. The Cambrian Period, in: Gradstein, F.M., Ogg,
1201 J.G., Schmitz, M.D., Ogg, G.M. (Eds.), Geologic Time Scale 2020. Elsevier, pp. 565–
1202 629. https://doi.org/10.1016/B978-0-12-824360-2.00019-X
1203 Peters, S.E., 2008. Environmental determinants of extinction selectivity in the fossil record.
1204 Nature 454, 626–629. https://doi.org/10.1038/nature07032
1205 Peters, S.E., 2006. Macrostratigraphy of North America. The Journal of Geology 114, 391–412.
1206 https://doi.org/10.1086/504176
1207 Peters, S.E., Husson, J.M., 2018. We need a global comprehensive stratigraphic database: here's
1208 a start. The Sedimentary Record 16, 4–9. https://doi.org/10.2110/sedred.2018.1.4

Peters, S.E., Husson, J.M., Czaplewski, J., 2018. Macrostrat: A Platform for Geological Data Integration and Deep-Time Earth Crust Research. Geochemistry, Geophysics, Geosystems 19, 1393–1409. https://doi.org/10.1029/2018GC007467

Peters, S.E., Quinn, D.P., Husson, J.M., Gaines, R.R., 2022. Macrostratigraphy: Insights into Cyclic and Secular Evolution of the Earth-Life System. Annual Review of Earth and Planetary Sciences 50, 419–449. https://doi.org/10.1146/annurev-earth-032320-081427

Peters, S.E., Walton, C.R., Husson, J.M., Quinn, D.P., Shorttle, O., Keller, C.B., Gaines, R.R., 2021. Igneous rock area and age in continental crust. Geology 49, 1235–1239. https://doi.org/10.1130/G49037.1

Petterson, R., Prave, A.R., Wernicke, B.P., Fallick, A.E., 2011. The Neoproterozoic Noonday Formation, Death Valley region, California. Geological Society of America Bulletin 123, 1317–1336. https://doi.org/10.1130/B30281.1

Pu, J.P., Bowring, S.A., Ramezani, J., Myrow, P., Raub, T.D., Landing, E., Mills, A., Hodgin, E., Macdonald, F.A., 2016. Dodging snowballs: Geochronology of the Gaskiers glaciation and the first appearance of the Ediacaran biota. Geology 44, 955–958. https://doi.org/10.1130/G38284.1

Quinn, D.P., Idzikowski, C.R., Peters, S.E., 2024. Building a multi-scale, collaborative, and time-integrated digital crust: The next stage of the Macrostrat data system. Geoscience Data Journal 11, 11–26. https://doi.org/10.1002/gdj3.189

Robert, B., Domeier, M., Jakob, J., 2021. On the origins of the Iapetus Ocean. Earth-Science Reviews 221, 103791. https://doi.org/10.1016/j.earscirev.2021.103791

Rooney, A.D., Cantine, M.D., Bergmann, K.D., Gómez-Pérez, I., Al Baloushi, B., Boag, T.H., Busch, J.F., Sperling, E.A., Strauss, J.V., 2020. Calibrating the coevolution of Ediacaran

life and environment. Proceedings of the National Academy of Sciences of the United States of America 117, 16824–16830. https://doi.org/10.1073/pnas.2002918117

Rooney, A.D., Strauss, J.V., Brandon, A.D., Macdonald, F.A., 2015. A Cryogenian chronology: Two long-lasting synchronous Neoproterozoic glaciations. Geology 43, 459–462. https://doi.org/10.1130/G36511.1

Schiffbauer, J.D., Bykova, N., 2024. Paleontology: Ediacaran ecology drove ocean ventilation. Current Biology 34, R734–R736. https://doi.org/10.1016/j.cub.2024.06.043

Schmitt, R.D.S., Fragoso, R.D.A., Collins, A.S., 2018. Suturing Gondwana in the Cambrian: The Orogenic Events of the Final Amalgamation, in: Siegesmund, S., Basei, M.A.S., Oyhantçabal, P., Oriolo, S. (Eds.), Geology of Southwest Gondwana, Regional Geology Reviews. Springer International Publishing, Cham, pp. 411–432. https://doi.org/10.1007/978-3-319-68920-3_15

Schmoker, J.W., Krystinik, K.B., Halley, R.B., 1985. Selected Characteristics of Limestone and Dolomite Reservoirs in the United States. AAPG Bulletin 69. https://doi.org/10.1306/AD4627F9-16F7-11D7-8645000102C1865D

Schoenborn, W.A., Fedo, C.M., Farmer, G.L., 2012. Provenance of the Neoproterozoic Johnnie Formation and Stirling Quartzite, southeastern California, determined by detrital zircon geochronology and Nd isotope geochemistry. Precambrian Research 206–207, 182–199. https://doi.org/10.1016/j.precamres.2012.02.017

Schrag, D.P., Higgins, John.A., Macdonald, F.A., Johnston, D.T., 2013. Authigenic Carbonate and the History of the Global Carbon Cycle. Science 339, 540–543. https://doi.org/10.1126/science.1229578

1254 Segessenman, D.C., Peters, S.E., 2024. Transgression–regression cycles drive correlations in
1255 Ediacaran–Cambrian rock and fossil records. Paleobiology 50, 150–163.
1256 https://doi.org/10.1017/pab.2023.31
1257 Segessenman, D.C., Peters, S.E., 2023. Macrostratigraphy of the Ediacaran System in North
1258 America, in: Laurentia: Whitmeyer, S.J., Williams, M.L., Kellett, D.A., Tikoff, B. (Eds.),
1259 Turning Points in the Evolution of a Continent. Geological Society of America, pp. 399–
1260 424. https://doi.org/10.1130/2022.1220(21)
1261 Servais, T., Cascales-Miñana, B., Harper, D.A.T., Lefebvre, B., Munnecke, A., Wang, W.,
1262 Zhang, Y., 2023. No (Cambrian) explosion and no (Ordovician) event: A single long-
1263 term radiation in the early Palaeozoic. Palaeogeography, Palaeoclimatology,
1264 Palaeoecology 623, 111592. https://doi.org/10.1016/j.palaeo.2023.111592
1265 Shahkarami, S., Buatois, L.A., Mángano, M.G., Hagadorn, J.W., Almond, J., 2020. The
1266 Ediacaran–Cambrian boundary: Evaluating stratigraphic completeness and the Great
1267 Unconformity. Precambrian Research 345, 105721.
1268 https://doi.org/10.1016/j.precamres.2020.105721
1269 Shi, W., Mills, B.J.W., Algeo, T.J., Poulton, S.W., Newton, R.J., Dodd, M.S., Zhang, Z., Zheng,
1270 L., He, T., Hou, M., Li, C., 2023. Heterogeneous sulfide reoxidation buffered oxygen
1271 release in the Ediacaran Shuram ocean. Geochimica et Cosmochimica Acta 356, 149–
1272 164. https://doi.org/10.1016/j.gca.2023.07.018
1273 Shields, G.A., Mills, B.J.W., Zhu, M., Raub, T.D., Daines, S.J., Lenton, T.M., 2019. Unique
1274 Neoproterozoic carbon isotope excursions sustained by coupled evaporite dissolution and
1275 pyrite burial. Nature Geoscience 12, 823–827. https://doi.org/10.1038/s41561-019-0434-
1276 3

1277 Shore, A.J., Wood, R.A., Butler, I.B., Zhuravlev, A.Yu., McMahon, S., Curtis, A., Bowyer, F.T.,
1278 2021. Ediacaran metazoan reveals lophotrochozoan affinity and deepens root of
1279 Cambrian Explosion. Science Advances 7, eabf2933.
1280 https://doi.org/10.1126/sciadv.abf2933
1281 Siscoe, G.L., Chen, C.-K., 1975. The paleomagnetosphere. Journal of Geophysical Research 80,
1282 4675–4680. https://doi.org/10.1029/JA080i034p04675
1283 Slagter, S., Konhauser, K.O., Briggs, D.E.G., Tarhan, L.G., 2024. Controls on authigenic
1284 mineralization in experimental Ediacara-style preservation. Geobiology 22, e12615.
1285 https://doi.org/10.1111/gbi.12615
1286 Slagter, S., Tarhan, L.G., Hao, W., Planavsky, N.J., Konhauser, K.O., 2021. Experimental
1287 evidence supports early silica cementation of the Ediacara Biota. Geology 49, 51–55.
1288 https://doi.org/10.1130/G47919.1
1289 Smith, E.F., Nelson, L.L., O'Connell, N., Eyster, A., Lonsdale, M.C., 2022. The
1290 Ediacaran−Cambrian transition in the southern Great Basin, United States. Geological
1291 Society of America Bulletin. https://doi.org/10.1130/B36401.1
1292 Smith, E.F., Nelson, L.L., Strange, M.A., Eyster, A.E., Rowland, S.M., Schrag, D.P.,
1293 Macdonald, F.A., 2016. The end of the Ediacaran: Two new exceptionally preserved
1294 body fossil assemblages from Mount Dunfee, Nevada, USA. Geology 44, 911–914.
1295 https://doi.org/10.1130/G38157.1
1296 Smith, M.D., Arnott, R.W.C., Ross, G.M., 2014. Physical and geochemical controls on
1297 sedimentation along an ancient continental margin: The deep-marine Old Fort Point
1298 Formation (Ediacaran), southern Canadian Cordillera. Bulletin of Canadian Petroleum
1299 Geology 62, 14–36. https://doi.org/10.2113/gscpgbull.62.1.14

1300 Soukup, M., Beranek, L.P., Lode, S., Goudie, D., Grant, D., 2024. Late Ediacaran to Early
1301 Cambrian Breakup Sequences and Establishment of the Eastern Laurentian Passive
1302 Margin, Newfoundland, Canada. American Journal of Science 324.
1303 https://doi.org/10.2475/001c.93038
1304 Sperling, E.A., Knoll, A.H., Girguis, P.R., 2015. The Ecological Physiology of Earth's Second
1305 Oxygen Revolution. Annual Review of Ecology, Evolution, and Systematics 46, 215–
1306 235. https://doi.org/10.1146/annurev-ecolsys-110512-135808
1307 Spero, H.J., Bijma, J., Lea, D.W., Bemis, B.E., 1997. Effect of seawater carbonate concentration
1308 on foraminiferal carbon and oxygen isotopes. Nature 390, 497–500.
1309 https://doi.org/10.1038/37333
1310 Sun, R., Shen, J., Grasby, S.E., Zhang, J., Chen, J., Yang, C., Yin, R., 2022. CO2 buildup drove
1311 global warming, the Marinoan deglaciation, and the genesis of the Ediacaran cap
1312 carbonates. Precambrian Research 383, 106891.
1313 https://doi.org/10.1016/j.precamres.2022.106891
1314 Swart, P.K., 2015. The geochemistry of carbonate diagenesis: The past, present and future.
1315 Sedimentology 62, 1233–1304. https://doi.org/10.1111/sed.12205
1316 Tan, Z., Luo, J., Xu, X., Jia, W., Li, J., Chen, L., 2024. New Re–Os Geochronological Data from
1317 the Upper Doushantuo Formation: Age Constraint on the Shuram Excursion and
1318 Implication for the Ediacaran Fluctuated Continental Weathering. ACS Omega 9, 49121–
1319 49131. https://doi.org/10.1021/acsomega.4c05072
1320 Tarhan, L.G., Hood, A. v.S., Droser, M.L., Gehling, J.G., Briggs, D.E.G., 2016. Exceptional
1321 preservation of soft-bodied Ediacara Biota promoted by silica-rich oceans. Geology 44,
1322 951–954. https://doi.org/10.1130/G38542.1

1323 Tasistro-Hart, A.R., Macdonald, F.A., 2023. Phanerozoic flooding of North America and the
1324 Great Unconformity. Proceedings of the National Academy of Sciences of the United
1325 States of America 120, e2309084120. https://doi.org/10.1073/pnas.2309084120
1326 Thomas, W.A., 1991. The Appalachian-Ouachita rifted margin of southeastern North America.
1327 Geological Society of America Bulletin 103, 415–431. https://doi.org/10.1130/0016-
1328 7606(1991)103<0415:TAORMO>2.3.CO;2
1329 Tian, X., Buck, W.R., 2022. Intrusions induce global warming before continental flood basalt
1330 volcanism. Nature Geoscience 15, 417–422. https://doi.org/10.1038/s41561-022-00939-w
1331 Tomkins, A.G., Martin, E.L., Cawood, P.A., 2024. Evidence suggesting that earth had a ring in
1332 the Ordovician. Earth and Planetary Science Letters 646, 118991.
1333 https://doi.org/10.1016/j.epsl.2024.118991
1334 Urey, H.C., 1952. On the Early Chemical History of the Earth and the Origin of Life.
1335 Proceedings of the National Academy of Sciences of the United States of America 38,
1336 351–363. https://doi.org/10.1073/pnas.38.4.351
1337 Valentine, J.W., Moores, E.M., 1970. Plate-tectonic Regulation of Faunal Diversity and Sea
1338 Level: a Model. Nature 228, 657–659. https://doi.org/10.1038/228657a0
1339 Van Staal, C.R., Zagorevski, A., 2023. Paleozoic tectonic evolution of the rifted margins of
1340 Laurentia, in: Whitmeyer, S.J., Williams, M.L., Kellett, D.A., Tikoff, B. (Eds.),
1341 Laurentia: Turning Points in the Evolution of a Continent. Geological Society of
1342 America, pp. 487–503. https://doi.org/10.1130/2022.1220(24)
1343 Wala, V.T., Ziemniak, G., Majka, J., Faehnrich, K., McClelland, W.C., Meyer, E.E., Manecki,
1344 M., Bazarnik, J., Strauss, J.V., 2021. Neoproterozoic stratigraphy of the Southwestern
1345 Basement Province, Svalbard (Norway): Constraints on the Proterozoic-Paleozoic

1346 evolution of the North Atlantic-Arctic Caledonides. Precambrian Research 358, 106138.
1347 https://doi.org/10.1016/j.precamres.2021.106138
1348 Waldron, J.W.F., Schofield, D.I., Murphy, J.B., 2019. Diachronous Paleozoic accretion of peri-
1349 Gondwanan terranes at the Laurentian margin. Geological Society of London Special
1350 Publications 470, 289–310. https://doi.org/10.1144/SP470.11
1351 Walton, C.R., Hao, J., Huang, F., Jenner, F.E., Williams, H., Zerkle, A.L., Lipp, A., Hazen,
1352 R.M., Peters, S.E., Shorttle, O., 2023. Evolution of the crustal phosphorus reservoir.
1353 Science Advances 9, eade6923. https://doi.org/10.1126/sciadv.ade6923
1354 Wang, H., Peng, Y., Li, C., Cao, X., Cheng, M., Bao, H., 2023. Sulfate triple-oxygen-isotope
1355 evidence confirming oceanic oxygenation 570 million years ago. Nature Communications
1356 14, 4315. https://doi.org/10.1038/s41467-023-39962-9
1357 Wang, R., Shen, B., Lang, X., Wen, B., Mitchell, R.N., Ma, H., Yin, Z., Peng, Y., Liu, Y., Zhou,
1358 C., 2023a. A Great late Ediacaran ice age. National Science Review 10, nwad117.
1359 https://doi.org/10.1093/nsr/nwad117
1360 Wang, R., Xing, C., Wen, B., Wang, X., Liu, K., Huang, T., Zhou, C., Shen, B., 2023b. The
1361 origin of cap carbonate after the Ediacaran glaciations. Global and Planetary Change 226,
1362 104141. https://doi.org/10.1016/j.gloplacha.2023.104141
1363 Wang, R., Yin, Z., Shen, B., 2023c. A late Ediacaran ice age: The key node in the Earth system
1364 evolution. Earth-Science Reviews 247, 104610.
1365 https://doi.org/10.1016/j.earscirev.2023.104610
1366 Wang, W., Li, C., Dodd, M.S., Algeo, T.J., Zhang, Z., Cheng, M., Hou, M., 2023. A DOM
1367 regulation model for dolomite versus calcite precipitation in the Ediacaran ocean:

1368 Implications for the “dolomite problem.” Precambrian Research 385, 106947.
1369 https://doi.org/10.1016/j.precamres.2022.106947
1370 Wang, X., Zhang, X., Zhang, Y., Cui, L., Li, L., 2021. New materials reveal Shaanxilithes as a
1371 Cloudina-like organism of the late Ediacaran. Precambrian Research 362, 106277.
1372 https://doi.org/10.1016/j.precamres.2021.106277
1373 Wei, G.-Y., Zhao, M., Sperling, E.A., Gaines, R.R., Kalderon-Asael, B., Shen, J., Li, C., Zhang,
1374 F., Li, G., Zhou, C., Cai, C., Chen, D., Xiao, K.-Q., Jiang, L., Ling, H.-F., Planavsky,
1375 N.J., Tarhan, L.G., 2024. Lithium isotopic constraints on the evolution of continental clay
1376 mineral factory and marine oxygenation in the earliest Paleozoic Era. Science Advances
1377 10, eadk2152. https://doi.org/10.1126/sciadv.adk2152
1378 Weil, A.B., Yonkee, A., 2023. The Laramide orogeny: Current understanding of the structural
1379 style, timing, and spatial distribution of the classic foreland thick-skinned tectonic
1380 system, in: Whitmeyer, S.J., Williams, M.L., Kellett, D.A., Tikoff, B. (Eds.), Laurentia:
1381 Turning Points in the Evolution of a Continent. Geological Society of America, pp. 707–
1382 771. https://doi.org/10.1130/2022.1220(33)
1383 Wilkinson, B., Walker, J.G.G., 1989. Phanerozoic Cycling of Sedimentary Carbonate. American
1384 Journal of Science 289, 525–548. https://doi.org/10.2475/ajs.289.4.525
1385 Williams, G.E., Schmidt, P.W., 2021. Dating the Acraman asteroid impact, South Australia: the
1386 case for deep drilling the ‘hot shock’ zone of the central uplift. Australian Journal of
1387 Earth Sciences 68, 355–367. https://doi.org/10.1080/08120099.2020.1808066
1388 Williams, H., King, A.F., 1979. Trepassey Map Area, Newfoundland. Geological Survey of
1389 Canada Memoir 389, 24 p.

1390 Willman, S., Peel, J.S., Ineson, J.R., Schovsbo, N.H., Rugen, E.J., Frei, R., 2020. Ediacaran
1391 Doushantuo-type biota discovered in Laurentia. Nature Communications Biology 3, 647.
1392 https://doi.org/10.1038/s42003-020-01381-7
1393 Wilson, J.T., 1966. Did the Atlantic Close and then Re-open? Nature 211, 676–681.
1394 https://doi.org/10.1038/211676a0
1395 Wong Hearing, T.W., Pohl, A., Williams, M., Donnadieu, Y., Harvey, T.H.P., Scotese, C.R.,
1396 Sepulchre, P., Franc, A., Vandenbroucke, T.R.A., 2021. Quantitative comparison of
1397 geological data and model simulations constrains early Cambrian geography and climate.
1398 Nature Communications 12, 3868. https://doi.org/10.1038/s41467-021-24141-5
1399 Wood, R., Liu, A.G., Bowyer, F., Wilby, P.R., Dunn, F.S., Kenchington, C.G., Cuthill, J.F.H.,
1400 Mitchell, E.G., Penny, A., 2019. Integrated records of environmental change and
1401 evolution challenge the Cambrian Explosion. Nat Ecology & Evolution 3, 528–538.
1402 https://doi.org/10.1038/s41559-019-0821-6
1403 Wu, C., Hua, H., Zeng, Z., Zheng, Y., Yang, D., Jiao, R., 2024. An Ediacaran glacial deposit in
1404 southern margin of the North China Craton: The Luoquan Formation—sedimentology,
1405 geochronology and provenance. Geological Journal 59, 2336–2363.
1406 https://doi.org/10.1002/gj.5022
1407 Xiao, S.H., Narbonne, G.M., 2020. The Ediacaran Period, in: Gradstein, F.M., Ogg, J.G.,
1408 Schmitz, M.D., Ogg, G.M. (Eds.), Geologic Time Scale 2020. Elsevier, pp. 521–561.
1409 https://doi.org/10.1016/B978-0-12-824360-2.00018-8
1410 Xu, D., Wang, X., Shi, X., Peng, Y., Stüeken, E.E., 2021. Feedback Between Carbon and
1411 Nitrogen Cycles During the Ediacaran Shuram Excursion. Frontiers in Earth Science 9,
1412 678149. https://doi.org/10.3389/feart.2021.678149

1413 Yang, C., Rooney, A.D., Condon, D.J., Li, X.-H., Grazhdankin, D.V., Bowyer, F.T., Hu, C.,
1414 Macdonald, F.A., Zhu, M., 2021. The tempo of Ediacaran evolution. Science Advances 7,
1415 eabi9643. https://doi.org/10.1126/sciadv.abi9643
1416 Ye, Y., Frings, P.J., Von Blanckenburg, F., Feng, Q., 2021. Silicon isotopes reveal a decline in
1417 oceanic dissolved silicon driven by biosilicification: A prerequisite for the Cambrian
1418 Explosion? Earth and Planetary Science Letters 566, 116959.
1419 https://doi.org/10.1016/j.epsl.2021.116959
1420 Youbi, N., Ernst, R.E., Mitchell, R.N., Boumehdi, M.A., El Moume, W., Lahna, A.A., Bensalah,
1421 M.K., Söderlund, U., Doblas, M., Tassinari, C.C.G., 2021. Preliminary Appraisal of a
1422 Correlation Between Glaciations and Large Igneous Provinces Over the Past 720 Million
1423 Years, in: Ernst, R.E., Dickson, A.J., Bekker, A. (Eds.), Geophysical Monograph Series.
1424 Wiley, pp. 169–190. https://doi.org/10.1002/9781119507444.ch8
1425 Zaffos, A., Finnegan, S., Peters, S.E., 2017. Plate tectonic regulation of global marine animal
1426 diversity. Proceedings of the National Academy of Sciences of the United States of
1427 America 114, 5653–5658. https://doi.org/10.1073/pnas.1702297114
1428 Zhang, F., Xiao, S., Romaniello, S.J., Hardisty, D., Li, C., Melezhik, V., Pokrovsky, B., Cheng,
1429 M., Shi, W., Lenton, T.M., Anbar, A.D., 2019. Global marine redox changes drove the
1430 rise and fall of the Ediacara biota. Geobiology 17, 594–610.
1431 https://doi.org/10.1111/gbi.12359
1432 Zhang, Y., Zhu, G., Li, X., Ai, Y., Duan, P., Li, M., Liu, J., 2024. Chemical–to–reverse
1433 weathering triggered a pronounced positive carbon isotope excursion in a forced
1434 regressive to transgressive dolostone succession during the terminal Ediacaran glaciation.

Global and Planetary Change 240, 104521. https://doi.org/10.1016/j.gloplacha.2024.104521

Zheng, K., Li, S., Gao, Y., Meng, W., Cheng, H., 2024. Advances in Reverse Weathering and Its Role in Clay Mineral Formation and the Carbon Dioxide Cycle. ACS Earth and Space Chemistry 8, 1680–1689. https://doi.org/10.1021/acsearthspacechem.4c00105

**Figure and Table Captions**

**Figure 1 –** Map of North America, Greenland (insert), and Svalbard (insert) with plotted areas of Ediacaran age stratigraphic columns colored by whether they contain carbonate or not (blue and gray, respectively) with locations of measured $\delta^{13}C$ and $\delta^{18}O$ compiled for this study (orange diamonds). Locations of geochemical measurements randomly jittered for visibility in high-density localities. Plotted Ediacaran stratigraphic data is from Segessenman and Peters, 2023.

**Figure 2 –** Time series of Ediacaran preserved sedimentary rock quantities and compiled carbonate $\delta^{13}C$ and $\delta^{18}O$ measurements anchored to rock quantity using a modified age model from Segessenman and Peters, 2023 with potentially relevant significant Ediacaran events highlighted. A full list of event timings and references can be found in Table 2. Three myr smoothing was applied to all rock quantity curves. Volume flux is reported in units of $km^3$/myr and area is reported in units of $km^2$. Carbonate quantities are split into three depositional environmental categories of nearshore, outer shelf, and slope/basin settings, in addition in an inferred marine category for carbonates with no clear environmental interpretation. A full list of carbonate rock units and their environmental interpretations from the published literature can be found in Table 1. A) volume flux, separated by depositional environment, and overlaid with raw

1459 $\delta^{13}C$ values; B) area of Ediacaran carbonates separated by depositional environment categories;
1460 C) volume flux of total marine siliciclastic and carbonate sedimentary rocks and counts of the
1461 number of sedimentary rock units through time; and D) area of total marine siliciclastic and
1462 carbonate sedimentary rocks and proportion of sedimentary rock units that have carbonate
1463 present.
1464
1465 **Figure 3 –** Time series of Ediacaran carbonate raw carbonate isotopic values and rock quantities
1466 split by phase (dolomite, calcite, and marble/unknown) and depositional environmental category
1467 (nearshore, outer shelf, and slope/basin) with potentially relevant significant Ediacaran events
1468 highlighted. A full list of event timings and references can be found in Table 2. Three myr
1469 smoothing was applied to all rock quantity curves. Volume flux is reported in units of $km^3$/myr
1470 and area is reported in units of $km^2$. A) time series of raw carbonate $\delta^{13}C$ values colored by
1471 phase; B) volume flux of limestone; C) volume flux of dolostone; D) area of limestone; E) area
1472 of dolostone.
1473
1474 **Figure 4 –** Time series of carbonate $\delta^{13}C$ averaged by locality, phase, and depositional
1475 environment category, and 5 myr moving window Spearman's ρ correlations between $\delta^{13}C$ and
1476 $\delta^{18}O$ values with potentially relevant significant Ediacaran events highlighted. A full list of event
1477 timings and references can be found in Table 2. Three myr smoothing was applied to all time
1478 series except that of locality. All averages were calculated with 3 myr moving window averages
1479 in which each relevant locality was averaged first, then the average of the locality averages was
1480 calculated to avoid biasing averages towards localities with greater sampling density. Bootstrap
1481 resampled error bars and confidence intervals were calculated and plotted for each time series.

A) $\delta^{13}C$ values averaged across localities; B) $\delta^{13}C$ values averaged by phase (calcite and dolomite); C) $\delta^{13}C$ values averaged by depositional environment category (nearshore, outer shelf, and slope/basin); and D) Spearman's ρ correlations between $\delta^{13}C$ and $\delta^{18}O$ values.

**Figure 5 –** Time series of carbonate raw $\delta^{18}O$ and averages separated by locality, phase, and depositional environment category with potentially relevant significant Ediacaran events highlighted. A full list of event timings and references can be found in Table 2. Three myr smoothing was applied to environmental and phase averages. All averages were calculated with 3 myr moving window averages in which each relevant locality was averaged first, then the average of the locality averages was calculated to avoid biasing averages towards localities with greater sampling density. Bootstrap resampled error bars and confidence intervals were calculated and plotted for each time series except the raw values plot. A) raw $\delta^{18}O$ values colored by depositional environment category (nearshore, outer shelf, and slope/basin); B) $\delta^{18}O$ values averaged by depositional environment category; C) $\delta^{18}O$ values averaged by locality; and D) $\delta^{18}O$ values averaged by phase (calcite and dolomite).

**Table 1 –** North American Ediacaran carbonate bearing unit names, their locality, their interpreted relative age, assigned depositional environment category for this study, the main interpretive statement from publications that supports our environmental category assignment, and the primary reference this evidence comes from.

**Table 2 –** Significant Ediacaran events highlighted on Figures 2-5, the timings/age ranges used for this study, relevant notes on interpretations of these events, and the publications that evidence and timings of the events can be found.

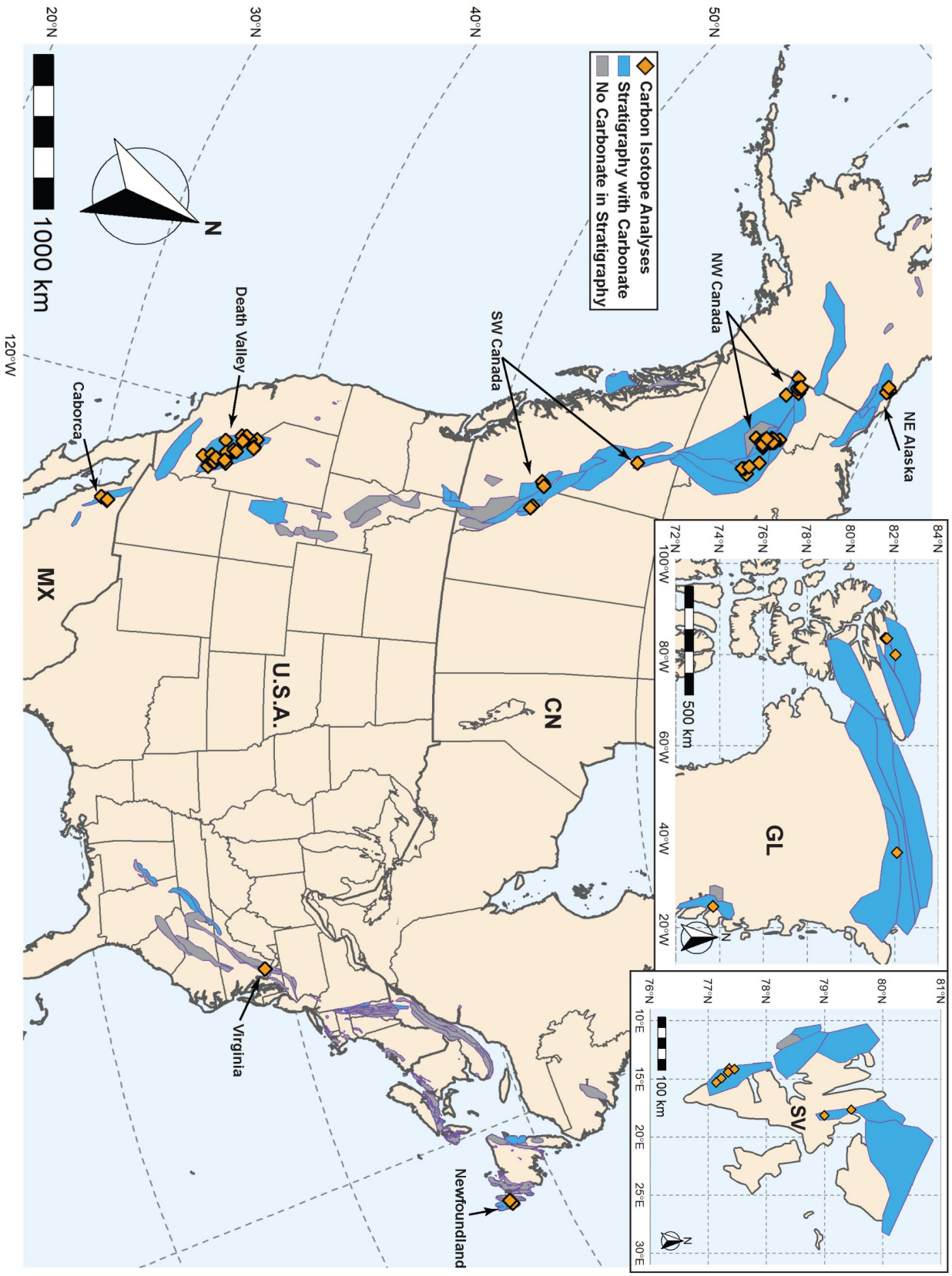
Carbon Isotope Analyses
Stratigraphy with Carbonate
No Carbonate in Stratigraphy
NW Canada
SW Canada
NE Alaska
Death Valley
Caborca
Virginia
Newfoundland
MX
U.S.A.
CN
GL
SV
N
1000 km
500 km
100 km
120°W
100°W
80°W
60°W
40°W
20°W
20°N
30°N
40°N
50°N
72°N
74°N
76°N
78°N
80°N
82°N
84°N
76°N
77°N
78°N
79°N
80°N
81°N
10°E
15°E
20°E
25°E
30°E

1507

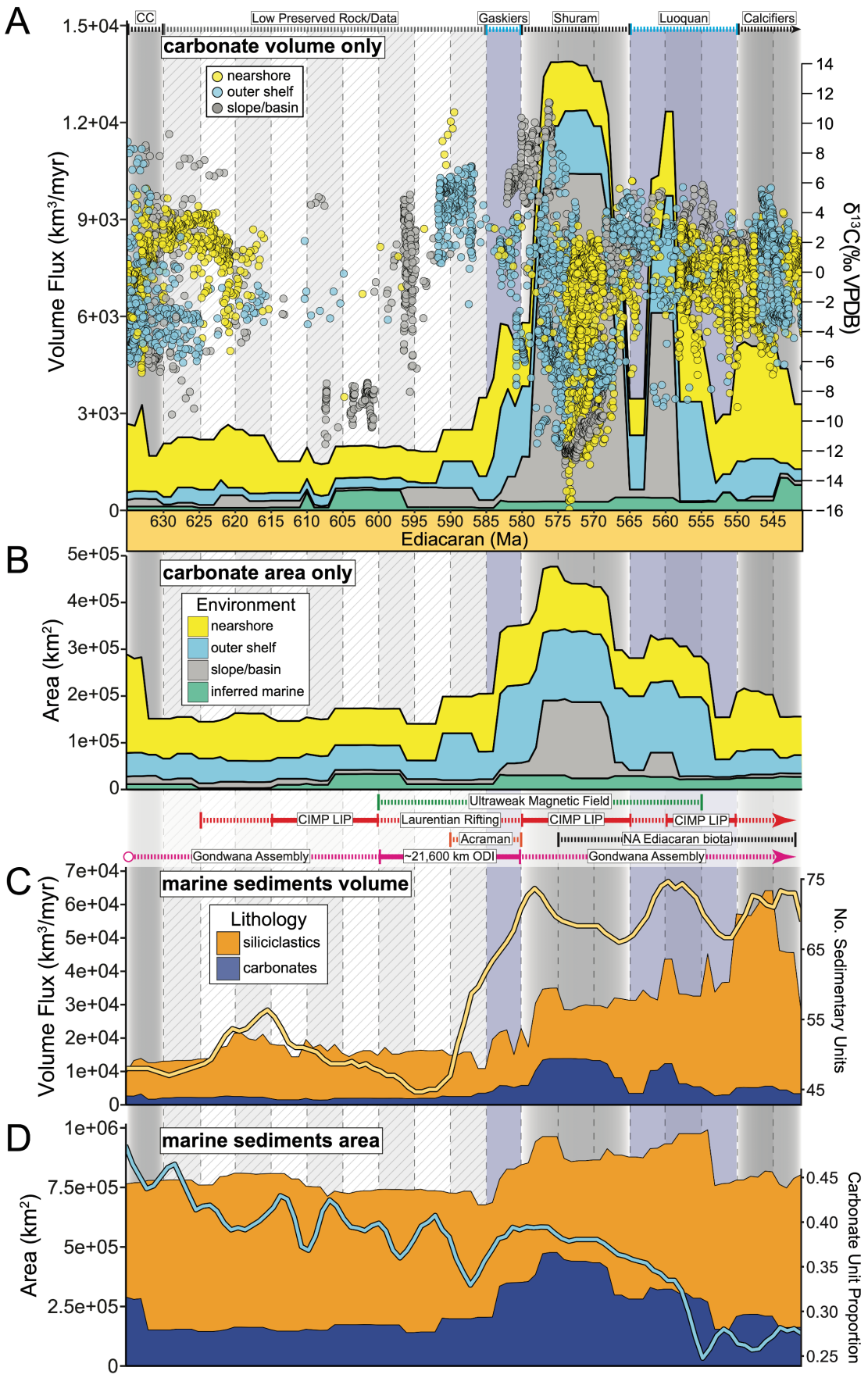
A
CC
Low Preserved Rock/Data
Gaskiers
Shuram
Luoquan
Calcifiers
carbonate volume only
nearshore
outer shelf
slope/basin
Volume Flux (km³/myr)
δ¹³C(‰ VPDB)
Ediacaran (Ma)
B
carbonate area only
Environment
nearshore
outer shelf
slope/basin
inferred marine
Area (km²)
Ultraweak Magnetic Field
CIMP LIP
Laurentian Rifting
CIMP LIP
CIMP LIP
Acraman
NA Ediacaran biota
Gondwana Assembly
~21,600 km ODI
Gondwana Assembly
C
marine sediments volume
Lithology
siliciclastics
carbonates
Volume Flux (km³/myr)
No. Sedimentary Units
D
marine sediments area
Area (km²)
Carbonate Unit Proportion

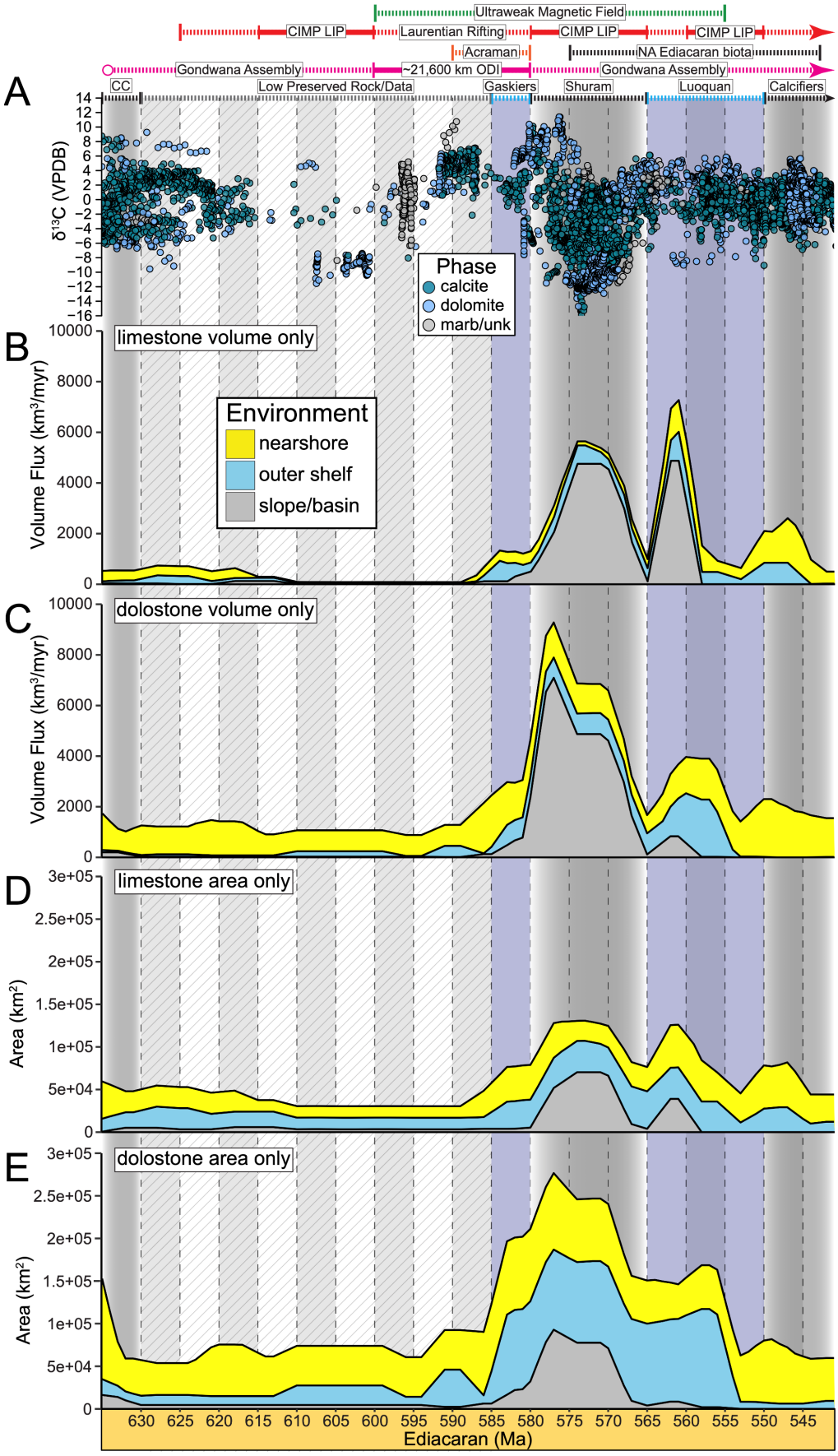
Ultraweak Magnetic Field
CIMP LIP
Laurentian Rifting
CIMP LIP
CIMP LIP
Acraman
NA Ediacaran biota
Gondwana Assembly
~21,600 km ODI
Gondwana Assembly
CC
Low Preserved Rock/Data
Gaskiers
Shuram
Luoquan
Calcifiers
A
δ13C (VPDB)
Phase
calcite
dolomite
marb/unk
B
limestone volume only
Volume Flux (km3/myr)
Environment
nearshore
outer shelf
slope/basin
C
dolostone volume only
Volume Flux (km3/myr)
D
limestone area only
Area (km2)
E
dolostone area only
Area (km2)
Ediacaran (Ma)

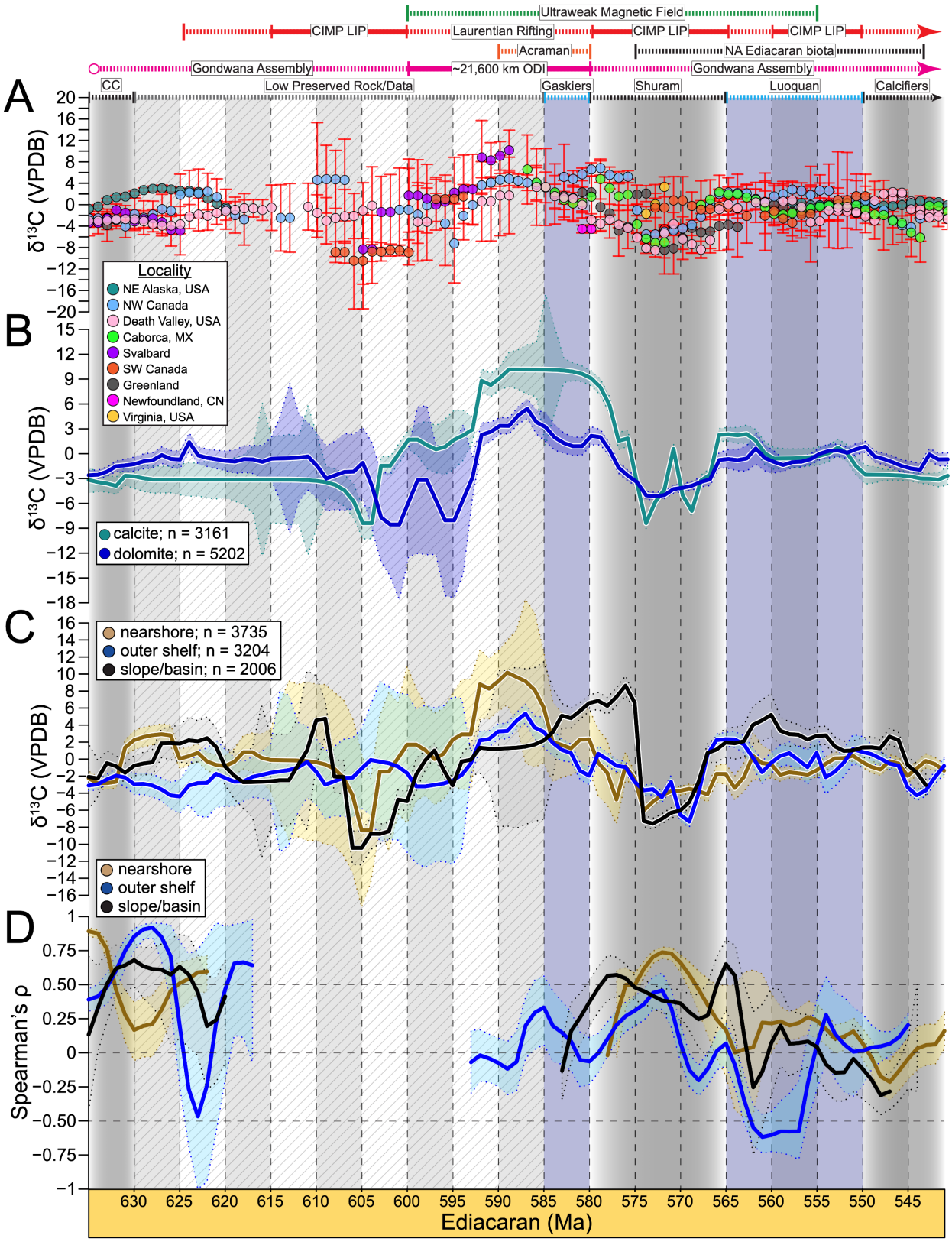
Ultraweak Magnetic Field
CIMP LIP
Laurentian Rifting
CIMP LIP
CIMP LIP
Acraman
NA Ediacaran biota
Gondwana Assembly
~21,600 km ODI
Gondwana Assembly
CC
Low Preserved Rock/Data
Gaskiers
Shuram
Luoquan
Calcifiers
A
δ13C (VPDB)
Locality
NE Alaska, USA
NW Canada
Death Valley, USA
Caborca, MX
Svalbard
SW Canada
Greenland
Newfoundland, CN
Virginia, USA
B
δ13C (VPDB)
calcite; n = 3161
dolomite; n = 5202
C
δ13C (VPDB)
nearshore; n = 3735
outer shelf; n = 3204
slope/basin; n = 2006
nearshore
outer shelf
slope/basin
D
Spearman's ρ
630 625 620 615 610 605 600 595 590 585 580 575 570 565 560 555 550 545
Ediacaran (Ma)

1510

1511

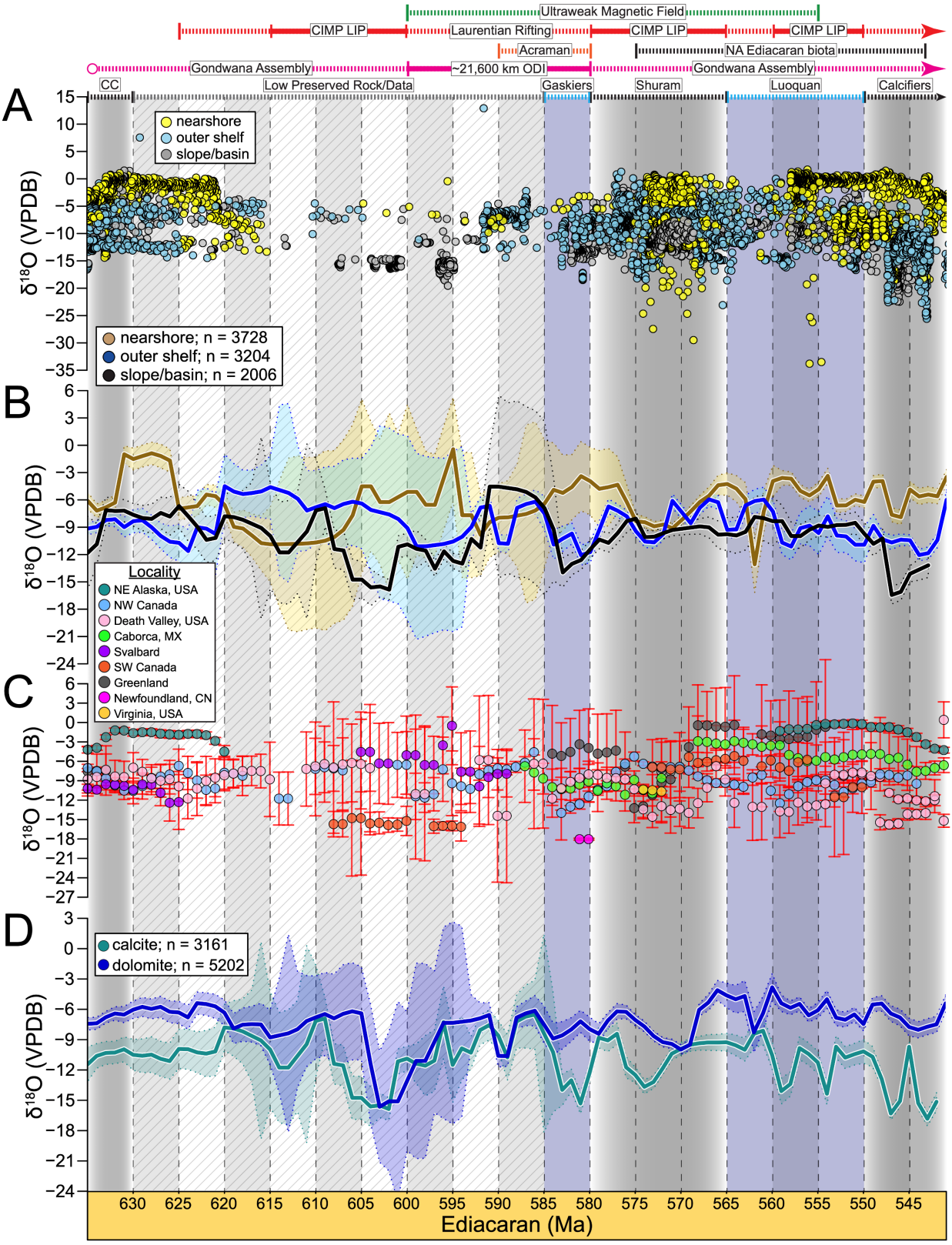
Ultraweak Magnetic Field
CIMP LIP
Laurentian Rifting
CIMP LIP
CIMP LIP
Acraman
NA Ediacaran biota
Gondwana Assembly
~21,600 km ODI
Gondwana Assembly
CC
Low Preserved Rock/Data
Gaskiers
Shuram
Luoquan
Calcifiers
A
nearshore
outer shelf
slope/basin
δ18O (VPDB)
nearshore; n = 3728
outer shelf; n = 3204
slope/basin; n = 2006
B
Locality
NE Alaska, USA
NW Canada
Death Valley, USA
Caborca, MX
Svalbard
SW Canada
Greenland
Newfoundland, CN
Virginia, USA
C
D
calcite; n = 3161
dolomite; n = 5202
630 625 620 615 610 605 600 595 590 585 580 575 570 565 560 555 550 545
Ediacaran (Ma)

1512

1513

| Carbonate Bearing Unit | Region | Interpreted Age | Environment Category | Main Interpretive Statement from Literature | Reference |
|---|---|---|---|---|---|
| Canyon Fm | Greenland | earliest Ediacaran | nearshore | forms the transgressive tract (cap dolostone) of the depositional sequence. The highstand tract culminates with shallow-water dolarenite | Hoffman et al., 2012 |
| Portfjeld Fm | Greenland | mid-late Ediacaran | nearshore | Typical facies include hummocky cross-stratified intraclast-rich grainstones and cherty dark dolostones of the mid- and outer ramp, and ooid–pisoid grainstones and varied microbial facies of the inner ramp | Willman et al., 2020 |
| Katakturuk Dolomite K2 | NE Alaska | earliest Ediacaran | slope/basin | Lower slope limestone rhythmites, turbidites, debris flows and shale | Macdonald et al., 2009 |
| Katakturuk Dolomite K2 | NE Alaska | earliest Ediacaran | nearshore | Back reef and ramp dolo-grainstone; Shoal complex dolo-microbialite | Macdonald et al., 2009 |
| Katakturuk Dolomite K3 | NE Alaska | early Ediacaran | nearshore | Back reef and ramp dolo-grainstone; Shoal complex dolo-microbialite | Macdonald et al., 2009 |
| Katakturuk Dolomite K3 | NE Alaska | early Ediacaran | slope/basin | Lower slope limestone rhythmites, turbidites, debris flows and shale | Macdonald et al., 2009 |
| Katakturuk Dolomite K4 | NE Alaska | latest Ediacaran | nearshore | Back reef and ramp dolo-grainstone | Macdonald et al., 2009 |
| Algae Fm | NW Canada | late Ediacaran | slope/basin | likely accumulated through a combination of hemipelagic carbonate sedimentation, sediment-gravity flows, and traction sedimentation as indicated by the sedimentary structures and depositional features | Moynihan et al., 2019 |
| Blueflower Fm | NW Canada | late Ediacaran | outer shelf | uppermost strata of the Blueflower Formation shoal gradationally into medium-bedded sandstone with hummocky cross stratification; transition from shelf to shoreface | Macdonald et al., 2013 |
| Blueflower Fm | NW Canada | late Ediacaran | slope/basin | mostly dominated by slope sedimentation. This is supported by the dominance of siliciclastic and mixed clastic-carbonate strata characterized by turbidites, slump folds, and soft-sediment deformation, and debris flow horizons | Moynihan et al., 2019 |
| Cliff Creek Fm | NW Canada | earliest Ediacaran | outer shelf | Fig. 12 of Busch et al., 2021 | Busch et al., 2021 |
| Fireweed Mbr | NW Canada | late Ediacaran | outer shelf | Fig. 12 of Busch et al., 2021 | Busch et al., 2021 |
| Gametrail Fm | NW Canada | late Ediacaran | slope/basin | The type Gametrail Formation is ~200 m thick and consists predominantly of thin-bedded limestone interbedded with massive carbonate debris flows and olistoliths | Macdonald et al., 2013 |
| Gametrail Fm | NW Canada | late Ediacaran | nearshore | inner ramp/reef complex/shoal complex | Busch et al., 2022 |
| Gladman Mbr | NW Canada | mid-late Ediacaran | outer shelf | Fig. 12 of Busch et al., 2021 | Busch et al., 2021 |
| Hayhook Fm | NW Canada | earliest Ediacaran | nearshore | interpreted correlative strata in the shallow-water Hayhook Formation in the Mackenzie Mountains | Cochrane et al., 2019 |
| Last Chance Mbr | NW Canada | late Ediacaran | outer shelf | Fig. 12 of Busch et al., 2021 | Busch et al., 2021 |
| Nadaleen Fm | NW Canada | upper Ediacaran | slope/basin | exhibits characteristic features of slope to basin floor sedimentation through a combination of suspension deposition and submarine sediment gravity flows | Moynihan et al., 2019 |
| Ravensthroat Fm | NW Canada | earliest Ediacaran | outer shelf | These strata most likely record hemipelagic carbonate sedimentation in a slope or outer-shelf setting | Moynihan et al., 2019 |
| Risky Fm | NW Canada | latest Ediacaran | nearshore | nearshore facies characterized by trough cross-bedded sandstone, stromatolites, oolitic grainstone, and paleokarst surfaces within the Risky Formation | Macdonald et al., 2013 |
| Sheepbed Carbonate | NW Canada | early Ediacaran | outer shelf | Exposures in the Wernecke Mountains clearly demonstrate that the Sheepbed carbonate is the HST deposit of Sequence 1 | Macdonald et al., 2013 |
| Sheepbed Fm | NW Canada | early Ediacaran | slope/basin | consists of >700m of siliciclastics deposited in a proximal to distal slope environment | Rooney et al., 2015 |
| Upper Rackla Gp | NW Canada | late Ediacaran | outer shelf | marine shelf | Macdonald et al., 2013 |
| Caborca Fm | NW Mexico | early Ediacaran | outer shelf | represent predominantly shallow marine carbonate and siliciclastic depositional environments generally no deeper than continental shelf depths | Loyd et al., 2012 |
| Clemente Fm | NW Mexico | mid-late Ediacaran | outer shelf | represent predominantly shallow marine carbonate and siliciclastic depositional environments generally no deeper than continental shelf depths | Loyd et al., 2012 |
| El Arpa Fm | NW Mexico | early Ediacaran | outer shelf | represent predominantly shallow marine carbonate and siliciclastic depositional environments generally no deeper than continental shelf depths | Loyd et al., 2012 |
| Gamuza Fm | NW Mexico | late Ediacaran | outer shelf | represent predominantly shallow marine carbonate and siliciclastic depositional environments generally no deeper than continental shelf depths | Loyd et al., 2012 |
| La Cienega | NW Mexico | latest Ediacaran | outer shelf | represent predominantly shallow marine carbonate and siliciclastic depositional environments generally no deeper than continental shelf depths | Loyd et al., 2012 |
| La Cienega | NW Mexico | latest Ediacaran | nearshore | shoreface to peritidal | Hodgin et al., 2021 |
| Paplote Fm | NW Mexico | late Ediacaran | outer shelf | represent predominantly shallow marine carbonate and siliciclastic depositional environments generally no deeper than continental shelf depths | Loyd et al., 2012 |
| Tecolote Fm | NW Mexico | late Ediacaran | outer shelf | represent predominantly shallow marine carbonate and siliciclastic depositional environments generally no deeper than continental shelf depths | Loyd et al., 2012 |
| Harbour Main Fm | SE Canada | mid-late Ediacaran | outer shelf | was probably inorganically precipitated and deposited well below the photic zone; lacks slope/basin structures | Myrow and Kaufman, 1999 |
| Fauquier Fm | SE USA | late Ediacaran | outer shelf | suggesting a shallower proximal marine to fluvial setting | Hebert et al., 2010 |
| Dracoisen Cap Carbonate | Svalbard | earliest Ediacaran | nearshore | forms the transgressive base of the Dracoisen cap carbonate sequence. The 3–15-m-thick, yellow to buff-weathering cap dolostone contains megaripples and peloids | Halverson et al., 2005 |
| Dracoisen Fm | Svalbard | early Ediacaran | nearshore | Above this level, the remainder of the Dracoisen consists mostly of mudcracked and ripple cross-laminated red and green siltstones | Halverson et al., 2004 |
| Hoferpynten Fm | Svalbard | earliest Ediacaran | outer shelf | finely laminated dolostone units that host distinct sedimentary structures, such as sheet crack cements, m-scale trochoidal bedforms, and finely laminated peloidal dolograinstone | Wala et al., 2021 |
| Slettfjelldalen Fm | Svalbard | earliest Ediacaran | outer shelf | finely laminated dolostone units that host distinct sedimentary structures, such as sheet crack cements, m-scale trochoidal bedforms, and finely laminated peloidal dolograinstone | Wala et al., 2021 |
| Isaac Fm | SW Canada | early-late Ediacaran | slope/basin | mixed carbonate-siliciclastic base-of-slope succession | Cochrane et al., 2019 |
| Matulka Gp | SW Canada | late Ediacaran | nearshore | A high-energy subtidal depositional setting associated with tidal sand bars and/or a migrating barrier complex | Eyster et al., 2018 |
| Old Fort Point Fm | SW Canada | early Ediacaran | slope/basin | variety of deep-marine processes in slope to basin-floor settings | Smith et al., 2014 |
| Dunfee Mbr | SW USA | late Ediacaran | nearshore | shallow marine to shoreface | Corsetti and Kaufman, 1994 |
| Dunfee Mbr | SW USA | late Ediacaran | outer shelf | consists of mixed carbonate-siliciclastic deposits representing slope to shallow subtidal settings | Smith et al., 2016 |
| Dunfee Mbr | SW USA | late Ediacaran | slope/basin | consists of mixed carbonate-siliciclastic deposits representing slope to shallow subtidal settings | Smith et al., 2016 |
| Esmeralda Mbr | SW USA | late Ediacaran | nearshore | green shoreface sandstone with mud cracks, interference ripples, and bed-planar trace fossils | Smith et al., 2016 |
| Johnnie Fm | SW USA | early-late Ediacaran | nearshore | contains mixed siliciclastic-carbonate lithofacies interpreted to represent shallow-marine deposition with minor fluvial influence | Corsetti and Kaufman, 2003 |
| Johnnie Fm | SW USA | mid-late Ediacaran | outer shelf | Proximal to distal reconstruction of Johnnie Fm from oolite to base of the Stirling | Bergmann et al., 2011 |
| Mahogany Flats Mbr | SW USA | early Ediacaran | nearshore | relatively uniform basinwide subsidence occurred during Mahogany Flats time, which was marked by deposition of stromatolitic and shallow-water dolostones | Petterson et al., 2011 |
| Noonday Dolomite | SW USA | early Ediacaran | outer shelf | interpreted to contain large domes (up to 200 m in diameter) interpreted as megastromatolites that approach the shelf margin | Corestti and Kaufman, 2003 |
| Radcliff Mbr | SW USA | earliest Ediacaran | nearshore | tidal marine; limestone rhythmites | Petterson et al., 2011 |
| Radcliff Mbr | SW USA | earliest Ediacaran | outer shelf | the distally steepened shelf succession, originally designated as the Ibex Formation Limestone and Shaley Limestone members | Creveling et al., 2016 |
| Reed Dolomite | SW USA | late Ediacaran | outer shelf | thickly bedded with no shallow/high-energy structures reported | Smith et al., 2023 |
| Sentinel Peak Mbr | SW USA | earliest Ediacaran | slope/basin | slope; sheet cracks and tubestone | Petterson et al., 2011 |
| Sitrling Quartzite | SW USA | late Ediacaran | nearshore | middle member of intertidal marine origin composed of dark gray platy siltstone, shale, and variable amounts of dolomite | Schoenborn et al., 2012 |
| Wood Canyon | SW USA | latest Ediacaran | nearshore | The lower and middle members of the Wood Canyon Formation record a shallow marine-continental braid-plain transition | Hagadorn and Waggoner, 2000 |
| Wyman Fm | SW USA | early-late Ediacaran | outer shelf | The section primarily represents shallow marine deposition; has trace fossils such Helminthoidichnites present | Corsetti and Hagadorn, 2000 |
| Yelverton Fm | N Canada | latest Ediacaran | outer shelf | shallow-marine carbonates (via Trettin, 1998) | Faehnrich et al., 2023 |

| Event | Timing/Age Range | Notes | Reference(s) |
|---|---|---|---|
| Laurentian Rifting | Late Tonian - Early Cambrian | North America western and eastern margins have overlapping but separate rift timings | Macdonald et al., 2023 and references therein |
| Central Iapetan Magmatic Province (CIMP) LIP | 615-600 Ma; 580-565; 560-550 Ma | see supplement of Condie et al., 2021 for detailed timings and evidence | Condie et al., 2021; Ernst et al., 2021; Robert et al., 2021; Youbi et al., 2021; Macdonald et al., 2023; Soukup et al., 2024 |
| Ultraweak Magnetic Field | 600-555 Ma | see highlighted UL-TAFI in Fig. 3 of Huang et al., 2024 | Domeier et al., 2023; Huang et al., 2024 |
| Acraman Impact Crater | 590-580 Ma | age based on Rb-Sr shale dating and chemmostratigraphy | Williams and Schmidt, 2021 |
| Gaskiers Glaciation | ?585-580 Ma | Pu et al., 2016 tightly constrained Gaskiers Fm glacial evidence, but Fitzgerald et al., 2024 discovered further evidence of glacial activity in underlying Mall Bay Fm. | Pu et al., 2016; Fitzgerald et al., 2024 |
| Shuram-Wonoka Excursion | 580-565 Ma | Timings from Rooney et al., 2020 and Cantine et al., 2024 provide tighter constraints assuming synchroneity; in this study our timing is also based on our age model | Rooney et al., 2020; Cantine et al., 2024 |
| North American Ediacaran Biota | ~575-539 Ma | Age range is a composite of many different fossil lineages and covers Avalon, White Sea, and Nama assemblages; youngest NA Ediacaran biota from SE USA | Xiao and Narbonne, 2020 and references therein |
| Gondwana Assembly | Early Ediacaran - Early Paleozoic | large number of orogenies associated with prolonged Gondwana supercontinent formation | Oriolo et al., 2017; Condie et al., 2021 |
| Major Orogenic Deformation Initiation (MODI) | 600-580 Ma | This refers to an anomalously increased (compared to preceding and following 10s of millions of years) length of orogenic fronts in which deformation initiates | Condie et al., 2021 and references therein |
| Luoquan Glaciation | ~565-550 Ma | Hankalchough and Luoquan formations both have proposed late Ediacaran glacial influence, we used Luoquan glaciation here due to Wu et al., 2024's tighter constraints | Wang et al., 2023a; Wang et al., 2023b; Wu et al., 2024 |
| Advent of Calcifying Metazoans | ~551-550 Ma | Age range given is for advent of metazoan (*Cloudina*) biomineralization, not the full duration of the earliest biomineralizers | Xiao and Narbonne, 2020; Bowyer et al., 2023 |